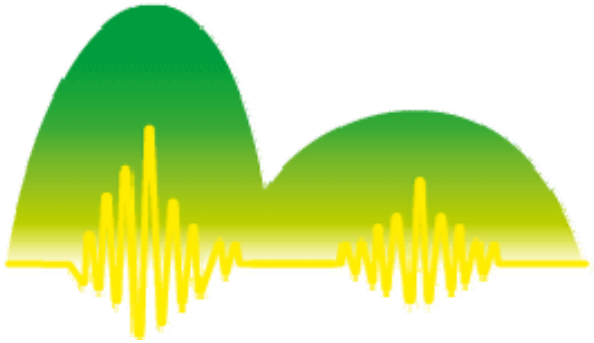

18th ISMAR MEETING
14th NMR USERS MEETING
Vth IBEROAMERICAN NMR MEETING
BIOMEDICAL IMAGING SYMPOSIUM
MAY 19-24, 2013 – RIO DE JANEIRO, RJ, BRAZIL
ROYAL TULIP RIO DE JANEIRO HOTEL

ISMAR & JHF

Jack H. Freed
Dept. of Chemistry and Chemical Biology
Cornell University
Ithaca, New York 14853 USA

ISMAR MEETINGS

- 1st Conference, 1962 (~~1965~~)- Tokyo, Japan
- 2nd Conference, 1965 (~~1968~~)- Sao Paulo, Brazil
- 3rd Conference, 1968 (~~1969~~)- Melbourne, Australia
* 4th Conference, 1971- Rehovot/Jerusalem, Israel
^ 5th Conference, 1974 - Bombay, India
* 6th Conference, 1977 - Banff, Alberta, Canada
* 7th Conference, 1980 - Delft, The Netherlands
* 8th Conference, 1983 - Chicago, Illinois USA
- 9th Conference, 1986 - Rio de Janeiro, Brazil
* 10th Conference, 1989 - Morzine, France
* 11th Conference, 1992 - Vancouver, Canada
* 12th Conference, 1995 - Sydney Australia
* 13th Conference, 1998 - Berlin, Germany
* 14th Conference, 2001 - Greek island of Rhodes
* 15th Conference, 2004 - Jacksonville, Florida USA
* 16th Conference, 2007 - Kenting, Taiwan
* 17th Conference, 2010 - Florence, Italy
* 18th Conference, 2013 - Rio de Janeiro, Brazil

* Meetings attended by JHF ^ TBD

1962: ISMAR: Tokyo, JAPAN

JHF: Receives Ph.D., Columbia University with G. K. Fraenkel

Ph.D. Thesis: A Study of Hyperfine Linewidths in ESR Spectra

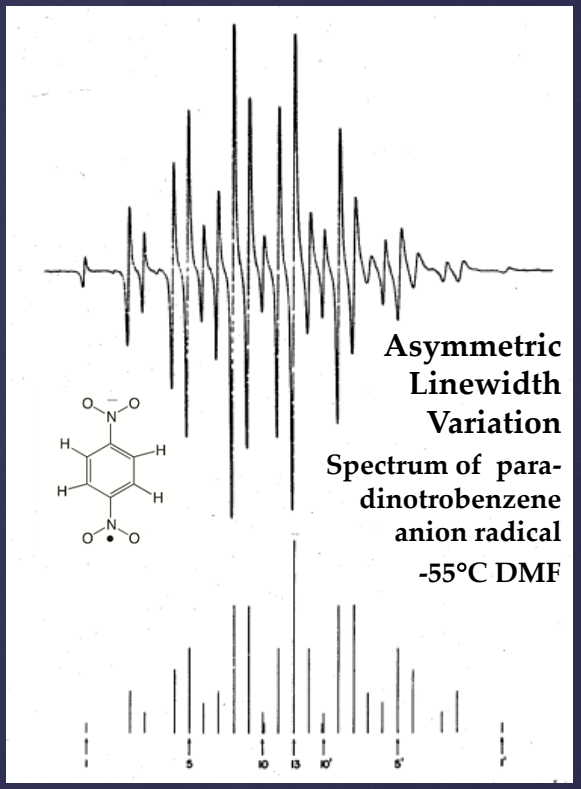

Alternating Linewidth - Spectrum of para-dinotrodurene anion radical in 20°C DMF

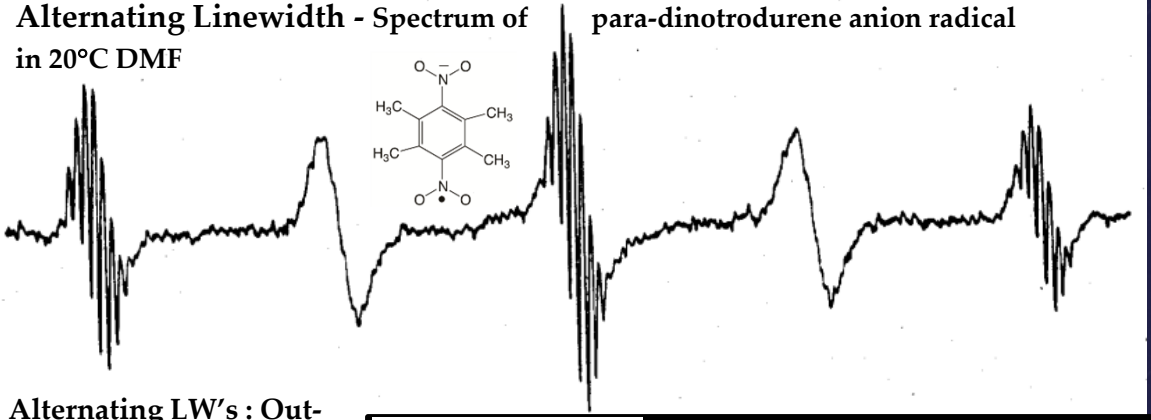

Alternating LW's : Out-of-phase correlation between the HF splittings of the two nitroxides in DND led to Equivalent Nuclei on Avg. vs. Completely Equivalent Nuclei.

Terms in the perturbation $\mathcal{H}_1(t)$.[a]

TABLE I. Terms in the perturbation $\mathcal{H}_1(t)$.[a]

		Dipolar: Isotropic (I)	Dipolar: Anisotropic (D)
$A_{\mu,i}^{(L,q)}$	$q=0$	$-\mathbf{I}_i\cdot\mathbf{S}$	$-2(\frac{2}{3})^{\frac{1}{2}}[I_{iz}S_z-\frac{1}{4}(I_{i+}S_-+I_{i-}S_+)]$
	$q=\pm1$	0	$\pm(I_{i\pm}S_z+I_{iz}S_\pm)$
	$q=\pm2$	0	$-I_{i\pm}S_\pm$
$F_{\mu,i}'^{(L,m)}(t)$		$\gamma_e[a_i(t)-\bar{a}_i]\delta_{m0}$	$(-1)^m\gamma_e\gamma_i\hbar D_i^{(m)}(t)$
			$D_i^{(m)}(t)=(6\pi/5)^{\frac{1}{2}}\langle\psi\mid r_i'^{-3}Y_{2m}(\theta_i',\phi_i')\mid\psi\rangle$

		g Tensor: Isotropic (G_0)	g Tensor: Anisotropic (G_2)
$A_{\mu,i}^{(L,q)}$	$q=0$	$-B_0S_z$	$-2(\frac{2}{3})^{\frac{1}{2}}B_0S_z$
	$q=\pm1$	0	$\pm B_0S_\pm$
	$q=\pm2$	0	0
$F_{\mu,i}'^{(L,m)}(t)$		$-\beta_e\hbar^{-1}[g_z(t)-\bar{g}_z]\delta_{m0}$	$-\frac{1}{2}(-1)^m\beta_e\hbar^{-1}g^{(m)}(t)$
			$g^{(0)}(t)=6^{-\frac{1}{2}}\{2g_3(t)-[g_1(t)+g_2(t)]\}$
			$g^{(\pm1)}(t)=0$
			$g^{(\pm2)}(t)=\frac{1}{2}[g_1(t)-g_2(t)]$

		Quadrupolar (Q)[b]: Anisotropic
$A_{\mu,i}^{(L,q)}$	$q=0$	$-(\frac{2}{3})^{\frac{1}{2}}[3I_{iz}^2-I_i(I_i+1)]$
	$q=\pm1$	$\pm(I_{i\pm}I_{iz}+I_{iz}I_{i\pm})$
	$q=\pm2$	$-I_{i\pm}^2$
$F_{\mu,i}'^{(L,m)}(t)$		$(-1)^m[eQ_i\hbar^{-1}[4I_i(2I_i-1)]^{-1}][\nabla\mathcal{E}(t)]_i^{(m)}$
		$[\nabla\mathcal{E}(t)]_i^{(0)}=-(\frac{2}{3})^{\frac{1}{2}}\langle\psi\mid V_{zz}'(i)\mid\psi\rangle$
		$[\nabla\mathcal{E}(t)]_i^{(\pm1)}=\pm\langle\psi\mid V_{xz}'(i)\pm iV_{yz}'(i)\mid\psi\rangle$
		$[\nabla\mathcal{E}(t)]_i^{(\pm2)}=-\frac{1}{2}\langle\psi\mid V_{xx}'(i)-V_{yy}'(i)\pm2iV_{xy}'(i)\mid\psi\rangle$

[a] The expressions for the $A_{\mu,i}^{(L,q)}$ are given in space-fixed axes while those for the $F_{\mu,i}'^{(L,m)}(t)$ are in the molecule-fixed axes coinciding with the principle values of the g tensor.
[b] Quadrupole moments are defined in the conventional manner. See, for example, Refs. 4, 21, or 39.

Necessitated New Paradigm for HF Linewidths in Organic Radicals: Freed – Fraenkel Theory:

Used Redfield Relaxation Matrix Based on WBR (Wangsness-Bloch-Redfield Theory) includes Degenerate HF Transitions. (JCP, 39, 326-48, 1963)

1965: ISMAR: San Paulo, Brazil
JHF: Assistant Professor, Cornell University

Theory of ESR Saturation and Double Resonance in Organic Free Radicals in Solution

ENDOR in Solution

Hyde & Maki, JCP 40, 3117 (1964)

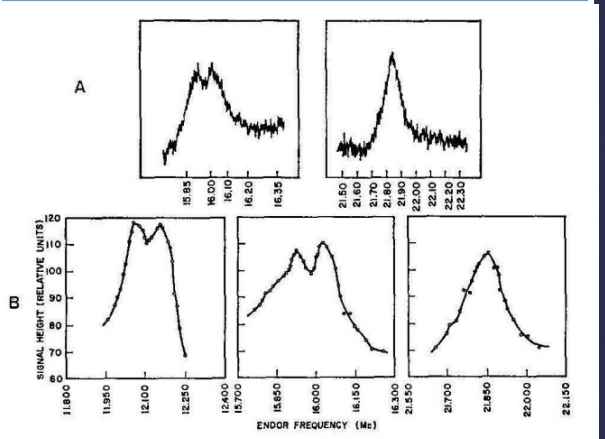

FIG. 1. Observed ENDOR Signals in Coppinger's radical.

Limiting Case of ENDOR from Theory

Freed, JCP 43, 2312 (1965)

TABLE II. Values of the enhancement factor E for several sets of values of transition probabilities when the $\omega_{aa'}$ and $\omega_{a'b'}$ transitions are excited.[a]

	a: $W_{x1}\sim W_{x2}=W_x$	b: $W_x=W_{x1}\gg W_{x2}$	c: $W_x=W_{x2}\gg W_{x1}$
(1) $W_e\sim W_n\sim W_x$	4/3	25/24	25/16
(2) $W_e\gg W_n\sim W_x$	1	1	1
(3) $W_n\gg W_e\sim W_x$	1	1	1
(4) $W_x\gg W_e\sim W_n$	$W_x/2(W_e+W_n)$	1	$W_x/(W_e+W_n)$
(5) $W_n\sim W_x\gg W_e$	3/2	1	2
(6) $W_e\gg W_x\gg W_n$	1	1	1
(7) $W_e\sim W_n\gg W_x$	9/8	9/8	9/8

[a] See Fig. 2.

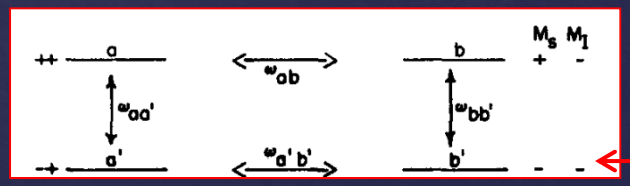

More General Application Of Redfield (WBR) Theory Leads To Coupled Solution In Matrix Form For The Many ESR Transitions In The Spectrum With Some Undergoing Saturation: Saturation Parameters Ωe,n

1968 ISMAR: Melbourne, Australia
JHF: Associate Professor, Cornell University

Electron-Electron Double Resonance (ELDOR)

with J. S. Hyde, J.C.W. Chien, JCP 48, 4211 (1968)

* Pump One Hyperfine Line and Observe Effect on Another HF Line

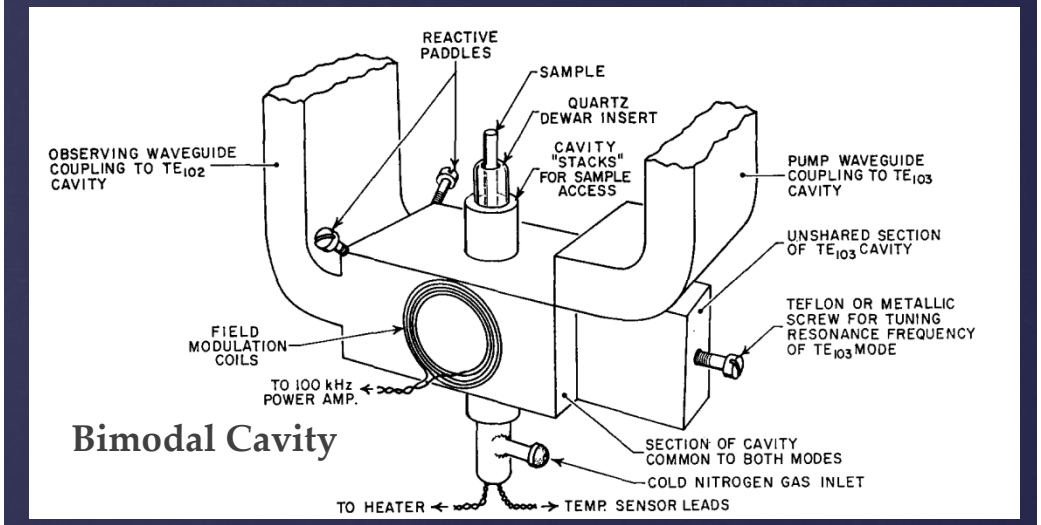

Bimodal Cavity

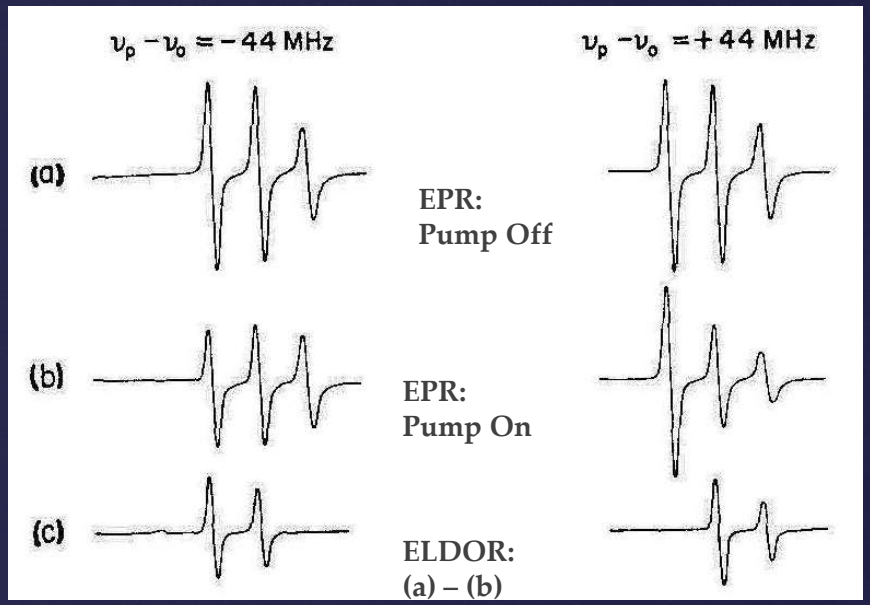

Nitroxide radical in ethybenzene, -80°C

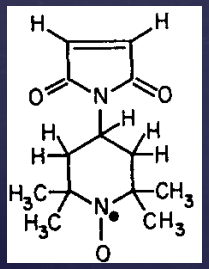

Nitroxide Radical

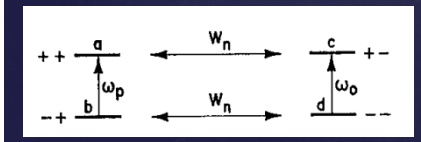

Reduction factor, *R*, for strongly saturated observing transition. $b = W_n / W_e$

Line pumped	Line observed: +1	0	−1
+1	···	$b/(1+3b)$	$b^2/(1+3b+2b^2)$
0	$(b+2b^2)/(1+4b+3b^2)$	···	$(b+2b^2)/(1+4b+3b^2)$
−1	$b^2/(1+3b+2b^2)$	$b/(1+3b)$	···

General Saturation & Double Res. Theory: ELDOR Reductions Depend on $\Omega_{o,p} \times \Omega_{p,o}$ the Cross-Saturation Parameters Between Observing and Pumped Transitions

1968 Cont.

Generalized Cumulant Expansions (GCE) and Spin-Relation Theory (JCP 49 376 (1968))

1. How to deal with break-down of WBR Theory Based on GCE method of Kubo.
2. Leads to Relaxation Matrix to all orders:

$$R = \sum_{n=1}^{\infty} R^{(n)}$$

for $t \gg \tau_c$ with $R^{(n)}$ of order $\left\langle \left| H_1^{\dagger}(t) \right|^n \right\rangle \tau_c^{n-1}$

3. This is a Complex Expansion in powers of $\left| H_1^{\dagger}(t) \right| \tau_c$

4. Also shows how to introduce "finite time" corrections when $\tau_c \gtrsim t$.

1971 ISMAR: Jerusalem, Israel
JHF: Attends (part of) ISMAR

The Stochastic Liouville Equation (SLE) and Slow Motional ESR (with G. Bruno and C.F. Polnaszek, JPC 75, 3385 (1971))

$$\frac{\partial \rho}{\partial t} = -i[\mathcal{H}(t), \rho]$$

ϱ : Spin Density Matrix
$\mathcal{H}(t)$: Random Hamiltonian

$$\frac{\partial}{\partial t} P(\Omega, t) = -\Gamma_{\Omega} P(\Omega, t)$$

P(Ω, t) : Probability of finding Ω at t .
Γ_{Ω} time independent Markoff Operator.

Leads to SLE:

$$\frac{\partial}{\partial t}\rho(\Omega,t) = -i[\mathcal{H}(\Omega),\rho(\Omega,t)] - \Gamma_{\Omega}\rho(\Omega,t)$$

$\rho(\Omega,t)$: Joint Spin Density Matrix As Well As Classical Probability Density in Ω.

- Kubo (1969) showed this with heuristic argument.
- Freed (1972) showed this with generalized moment expansion.
- Hwang & Freed (1975) developed this by passing to semi-classical limit from quantum stat. mech. Leads to a "spin-force" and/or "spin-torque" back-reaction of spins on bath. Confirms high T limit.
- Wassam & Freed (1982) developed this from even more general many-body quantum stat. mech.

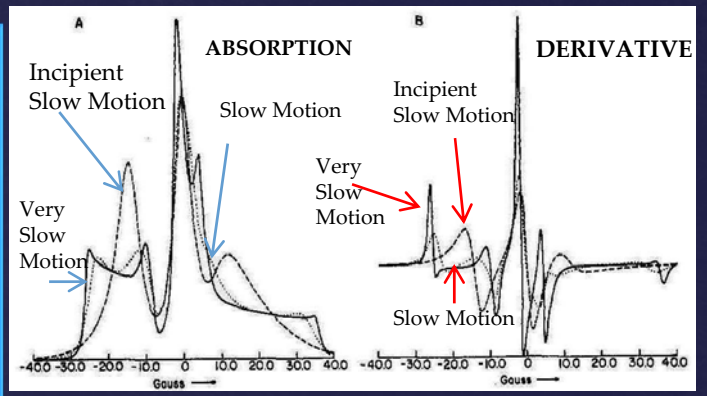

Line Shapes for $S = \frac{1}{2}$, $I = 1$ (^{14}N nucleus) with axially symmetric g tensor, hyperfine tensor, and small ω_n.

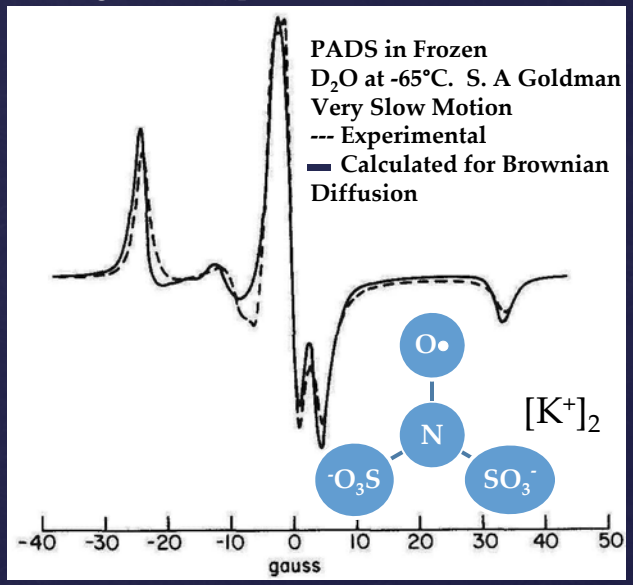

1974 : ISMAR: Bombay, India

JHF: Did not receive letter from India with invitation to deliver plenary lecture.

Studies of Electron Spin Relaxation of Nitroxide Probes in Solution: Fast & Slow Motions and Search for a Model, (with J. Hwang, R. Mason and L.-P. Hwang, JPC 79, 489 (1975))

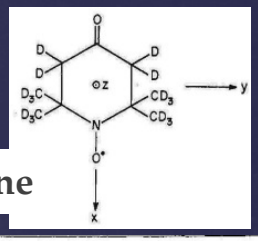

PD-Tempone

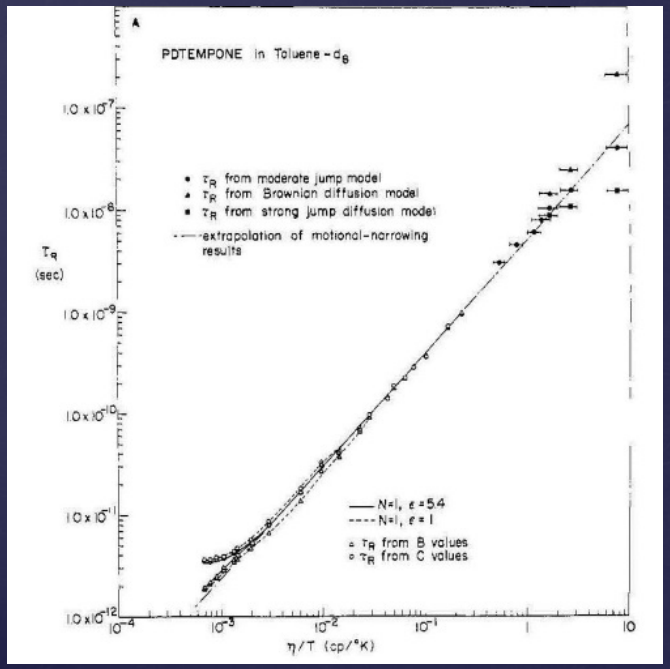

τ_R vs. η/T over five orders of magnitude

Non-secular spectral densities:
$j(\omega) \approx \tau_R/[1+\varepsilon\omega^2\tau_R^2]^{-1}$, $\varepsilon > 1$

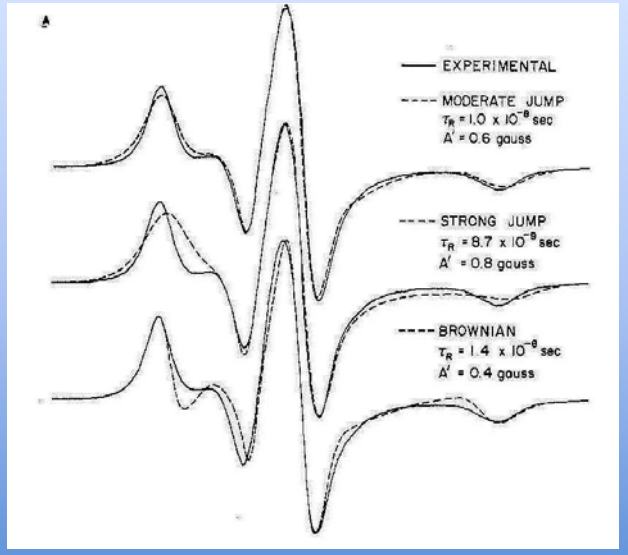

Comparison of experiment and simulated spectra in the model-dependent slow-tumbling region for PD-Tempone in toluene-d_8

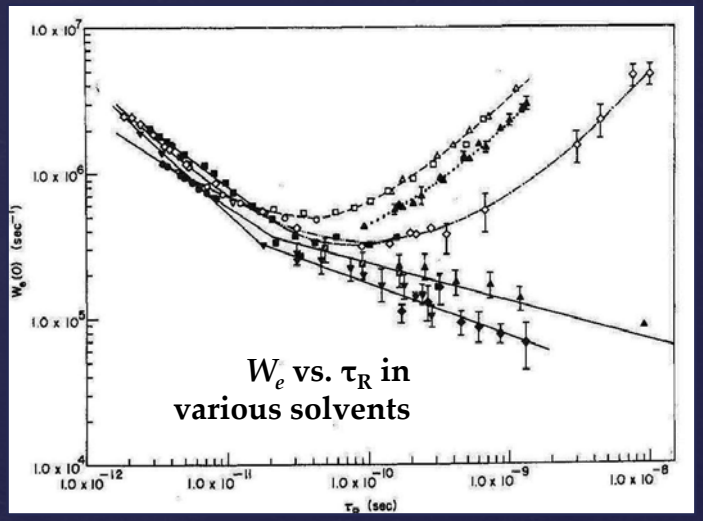

W_e vs. τ_R in various solvents

Brownian vs. Jump Diffusion: Slow Motional Fits.

Fluctuating Torques (Fast Bath Modes) vs. Slowly Relaxing Structures (Slow Bath Modes)

1977: ISMAR: Banff, Canada
JHF: Lectures

ESR and Spin Relaxation in Liquid Crystals (with C.F. Polnaszek, JPC 79 2282, (1975))

Liquid Crystals Yield an Anisotropic Environment:

$$P_o(\Omega) = \exp(-U(\Omega)/kT) \Big/ \int d\Omega \exp(-U(\Omega)/kT)$$

U(Ω) : Anistropic Potential

A challenge to diagonalization: Leads to non-symmetric matrices. Render symmetric by similarity transformation:

$$\tilde{P}(\Omega,t) \equiv P_0(\Omega)^{-1/2} P(\Omega,t)$$

Symmetrized Diffusion Operator:

$$\tilde{\Gamma} = M \bullet R \bullet M + \frac{M \bullet R \bullet MU}{2\kappa T} + \frac{T \bullet R \bullet T}{(2\kappa T)^2}$$

M: Vector Operator which generates an infinitesimal Rotation.

T ≡ iMU(Ω) is the external torque derived from the potential U(Ω).

Yielding: $\partial \tilde{P} / \partial t = -\tilde{\Gamma}_\Omega \tilde{P}(\Omega,t)$

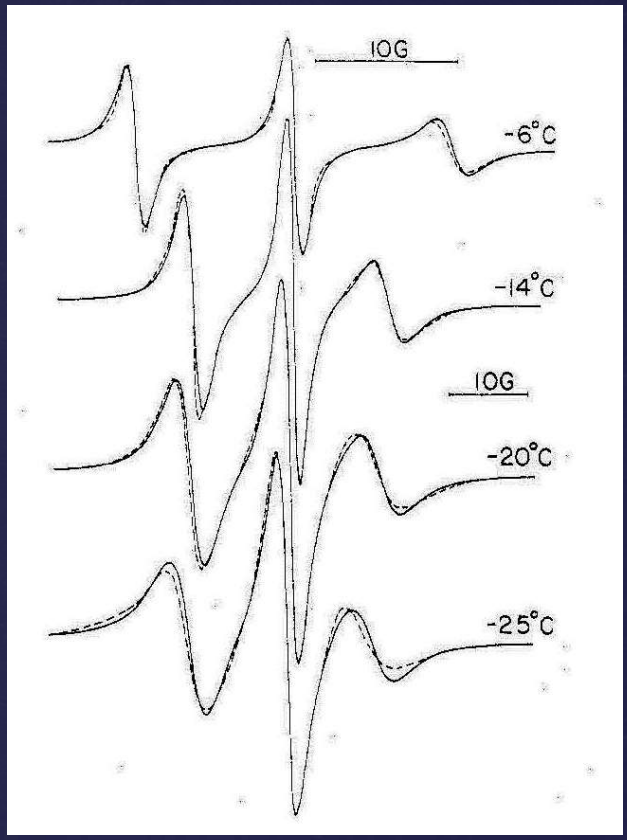

Comparison of experimental (-----) and theoretical (——) spectra for PD-Tempone in Phase V stresses the need for SRLS model.

1977 Cont.

High Pressure (J.S. Hwang and K.V.S. Rao, JPC 80, 1490 (1976))

More evidence for SRLS from High Pressure Experiments

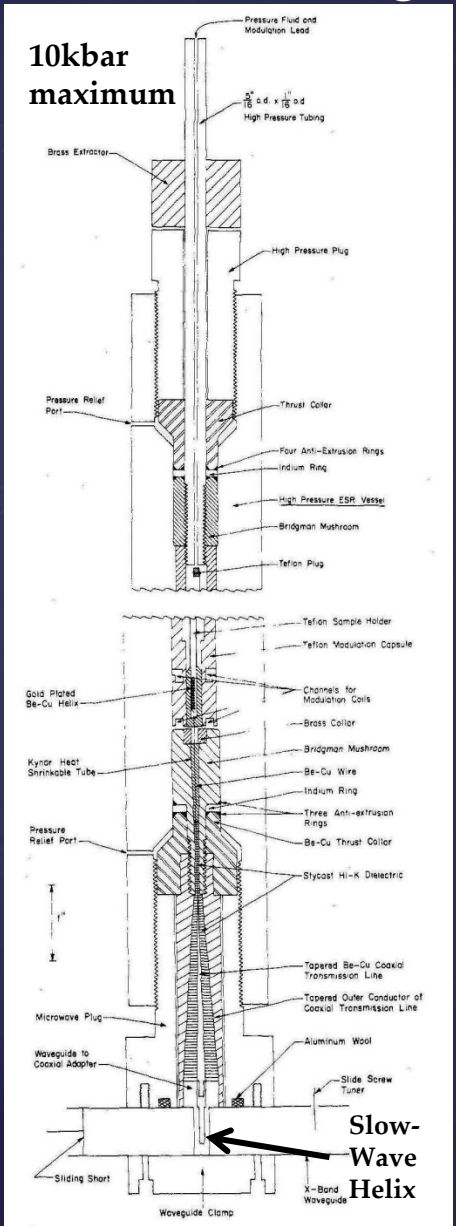

ESR High Pressure Vessel (Hydraulic)

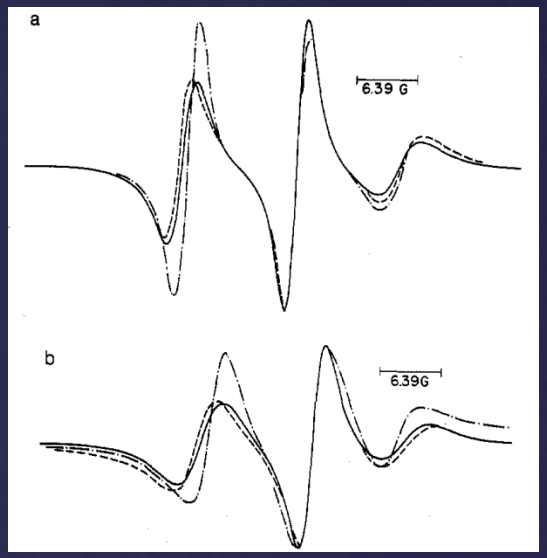

Comparison of experimental and simulated spectra at 45°C for PD-Tempone in Phase V (a) 3450 bars (b)4031 bars (- - - -) experimental results; (· - · - ·) and (▬) theoretical results for different models.

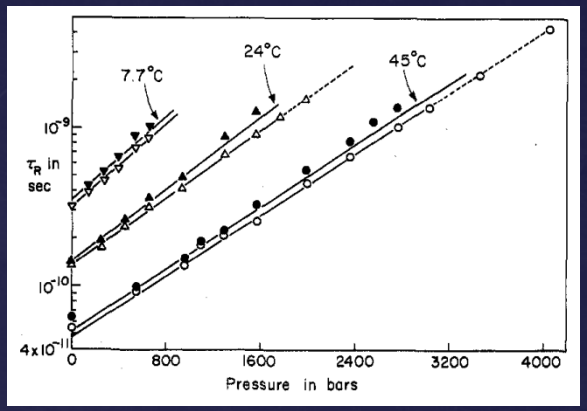

Graph of τ_R vs. pressure for PD Tempone in phase V.

General Theoretical Analysis Led to Expressions for SRLS Spectral Density (JCP, 66, 483 (1977):

$$J_{KM}(\omega) = \frac{\kappa(K,M)\tau_R}{1+\omega^2\tau_R^2} + \tfrac{1}{5}[5\kappa(0,M)]^2\,\delta_{K,0}\langle|S_l|^2\rangle \times\left[\frac{\tau_x}{1+\omega^2\tau_x^2} - \frac{\tau'_R}{1+\omega^2\tau_R'^2}\right]$$

Where $\tau_R'^{-1} = \tau_R^{-1} + \tau_x^{-1}$ and κ=1/5 for isotropic medium. Later referred to as "Model Free" expression.

1980 ISMAR : Delft, Netherlands

JHF: In attendance, but barred from presenting.

Efficient Computation of ESR Spectra and Related Fokker-Planck Forms by the Use of the Lanczos Algorithm (LA)

(with Giorgio Moro, JCP 74 , 3757 (1981))

Spectrum from SLE:

$$I(\omega) = \frac{1}{\pi} \mathrm{Re}\{ < \nu | \, [\mathrm{i}(\omega 1 - \mathcal{L}) + \Gamma]^{-1} \, | \nu > \}$$

$\mathcal{L}$ - Liouville operator associated with spin Hamiltonian

Γ - Symmetrical diffusion operator

$|\nu>$ - Vector of allowed spectral components

The Lanczos algorithm : Let $A \equiv \Gamma + iL$
By operating with A n times on $|\nu>$ and simple rearranging, an n-dimensional orthonormal sub-set of the N >> n total basis set is obtained such that A_n is tri-diagonal with $A_n = P_n A P_n^{-1}$ where P_n projects out the "Relevant Sub-Space."

Distribution of the eigenvalues for calculation. Units are in G; x & y axis represent real & imaginary parts of the eigenvalues. △ from Lanczos algorithm; • exact.

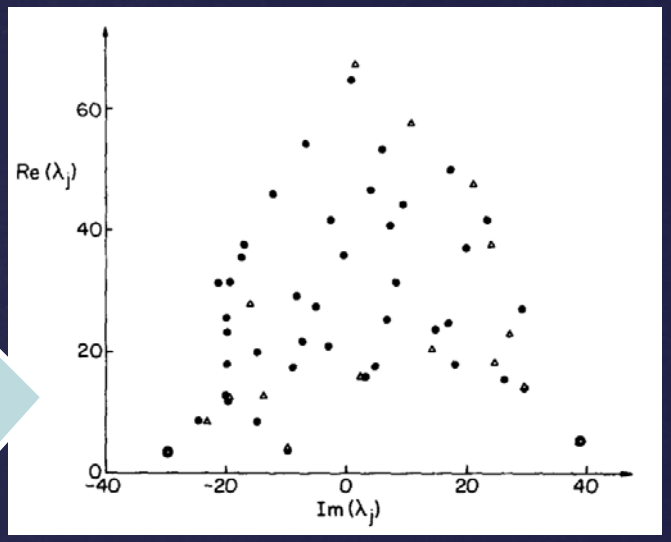

This was the first significant application of the LA to Complex Symmetric (non-Hermitian) Matrices.
Leads to Order(s) of Magnitude Reduction in Computer Space &Time.

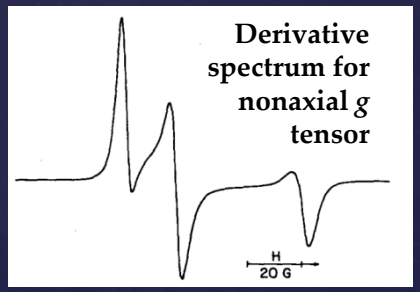

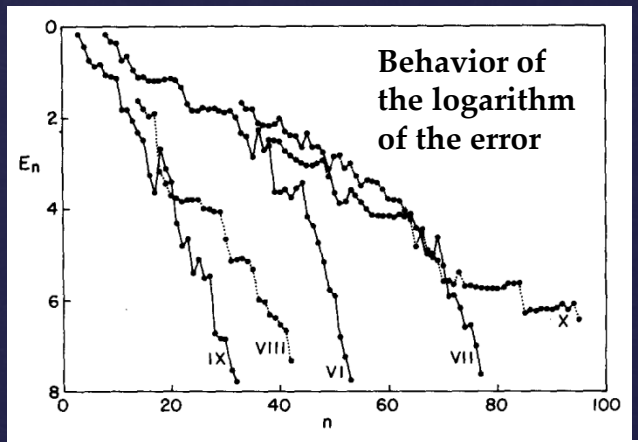

Lanczos Steps rapidly converge to solution

1980 cont.

- The computational algorithm is formally equivalent to the Mori Method in Statistical Mechanics: i.e. in projecting out the relevant sub-space:
- But in the Mori method, general arguments are given for the many-body problem, while we used the SLE approximation to the many-body problem but with a well-defined computational methodology.

General Conclusion:

The Quantum World with its Microscopic Reversibility is Represented by Unitary Space.

But the Real World with its Irreversibility is Properly Represented by (complex) – Orthogonal Space.

Suppose one starts with an arbitrary matrix representation with both coherence and damping: M

THEOREM:

Equivalent to a complex symmetric matrix through a similarity transformation: $A=SMS^{-1}$ i.e. where A is complex symmetric and $S \equiv UH$ where H is Hermitian and U is Unitary.

This we accomplish with a diagonal Hermitian Matrix: $H \rightarrow P_o^{1/2}(\Omega)$ and U→ Transforms the basis set to be time reversal invariant. Then both $\mathcal{L}$ and Γ are represented by real symmetric matrices. (cf. D. Schneider and J.H.F. 1989).

This methodology permitted calculating ESR spectra for smectic liquid crystals where the normal to the smectic planes is tilted relative to the magnetic field destroying the cylindrical symmetry.

1983 ISMAR: Chicago
JHF: Lectures

Nuclear Spin Waves in (Doubly) Spin-Polarized Atomic Hydrogen Gas

(with B.R. Johnson, J.S. Denker, N. Bigelow, L.P. Levy, D.M. Lee, PRL 52, 1508, 1984)

Spin-polarized H↓ is a gas of atomic hydrogen with the electron spins aligned by cooling the H atoms to T < 0.5K in a magnetic field H = 8 – 10 Tesla. Thus pairwise collisions of pure H ↓ atoms cannot recombine due to the Pauli Exclusion Principle (S = 1).

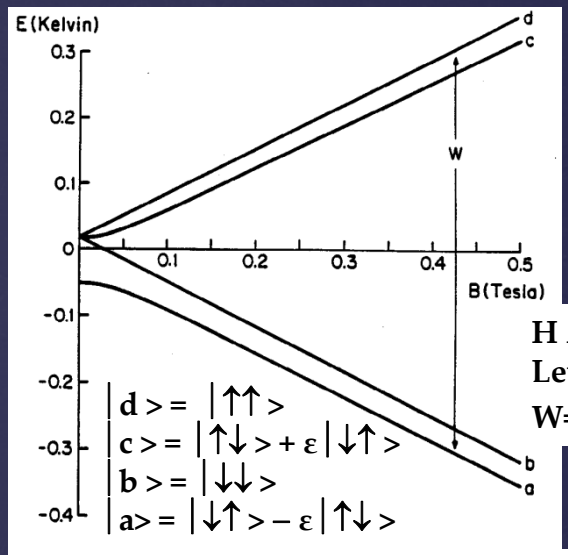

H Atom Energy Levels

W= 10K at 8T

Yet it is nearly an ideal gas: PV = nRT ! as well as a gas of Bosons.

But nuclear spin polarization requires T < 30 mK at 10 Tesla. Thus both ground state |a> and next state |b> are initially populated.

But |a> is not a pure state:

$|a> = |{\downarrow\uparrow}> - \varepsilon\,|{\uparrow\downarrow}>$ $\quad \varepsilon = a/2\gamma_e B_0$

At 10 Tesla $\varepsilon \cong 2.5 \times 10^{-3}$

This provides a recombination pathway.

In time, only the |b> = |↓↓> state remains a pure state of doubly spin-polarized H↓ ↓

For $10^{16} – 10^{17}$ atoms/cm^3

- Nuclear T_1 ~ hours
- Recombination times for |a> ~ 2 – 10 min.

Lengths:

- S-wave scattering length between 2H↓ atoms: $a_s \cong 0.72$Å
- thermal de Broglie wavelength $\lambda_T \cong$ 20-50Å
- spin-wave wavelength λ ~ 0.1 – 1.0 cm
- sample size L = 0.6 X 1.0 cm.

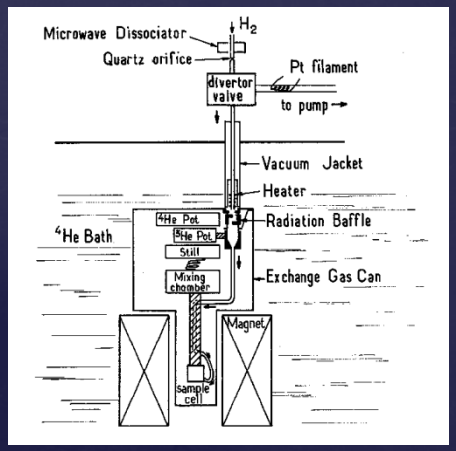

Schematic Diagram of cryostat & atomic hydrogen source

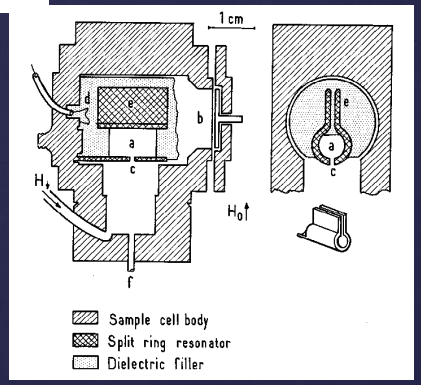

The sample cell with "loop-gap" or split ring resonator. Surfaces coated with saturated film of superfluid ^{4}He.

1983 Cont.

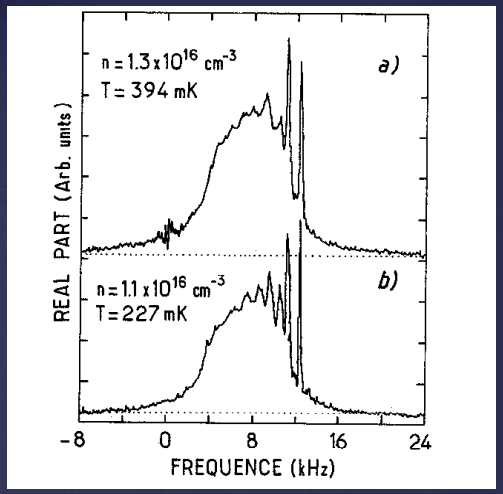

FT-NMR spectra for H↓↓ at 2 temperatures

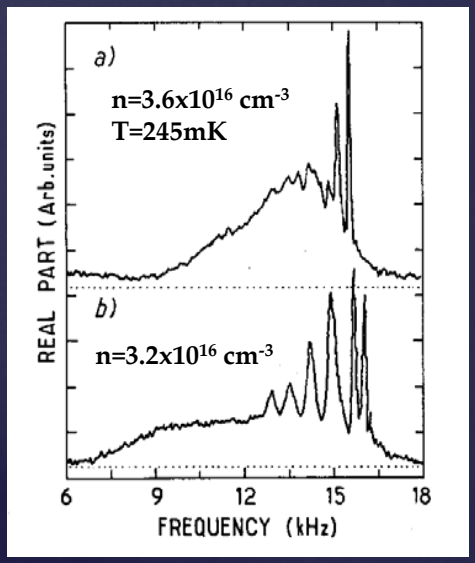

FT-NMR spectra for H↓↓ at 2 gradients. b) larger gradient than a)

Spin Waves due to apparent nuclear-spin-dependent collision cross-section of H ↓↓ . This is an effect of the Bose statistics on the nuclear degrees of freedom. True interaction potential is just that of the electron-spin triplet potential energy curve.

For small tipping angles:

$$i\frac{\partial \tilde{P}_+}{\partial t} = i\hat{D}\,\nabla^2\tilde{P}_+ + \gamma\delta H_0(\mathbf{r})\,\tilde{P}_+$$

$$\hat{D} = D\frac{(1 - i\varepsilon\mu P_z)}{1 + \mu^2 P^2}$$

Quality factor:

$$\mu = \frac{\lambda_T}{a_s}$$

ε = 1 for Bosons

$\hat{D}$ is complex effective diffusion coefficient

P is nuclear spin polarization with components P_+ & P_z

In absence of gradient: simple standing waves.
With gradient: Can solve for the complex eigenvalues: Airy Fns.

The act of using a field gradient to image the spin waves traps the modes by the "linear potential well"

Find $P_z = 0.9 \pm 0.1$

$\mu T^{1/2} = 3.5 \pm 0.4$ (Thy: 3.65)

$nD_o = 1.3 \times 10^{18}$ cm^{-1}sec^{-1}

(Thy: 1.5×10^{18} cm^{-1}sec.$^{-1}$)

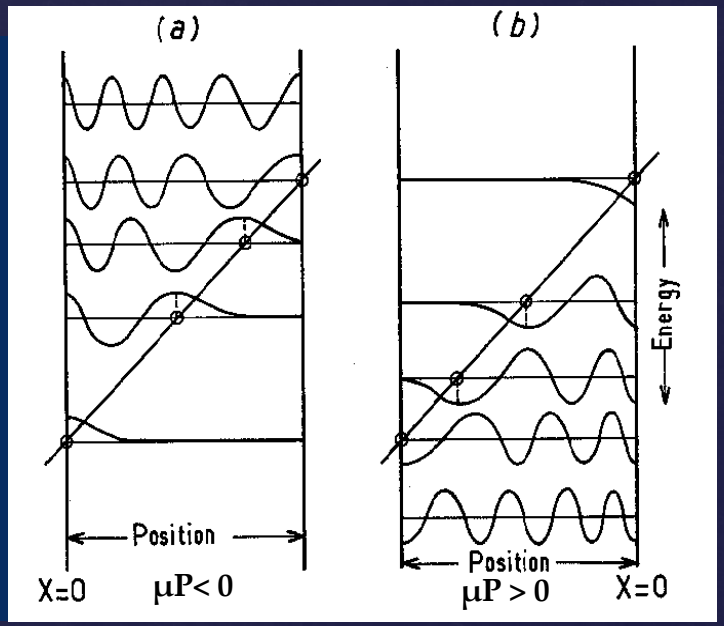

1986 ISMAR: Rio de Janiero
JHF: Did not attend

Two-Dimensional Fourier Transform ESR: 2D-ELDOR (with Jeff Gorcester,

JCP 85, 5375 (1986); 88, 4678 (1988).)

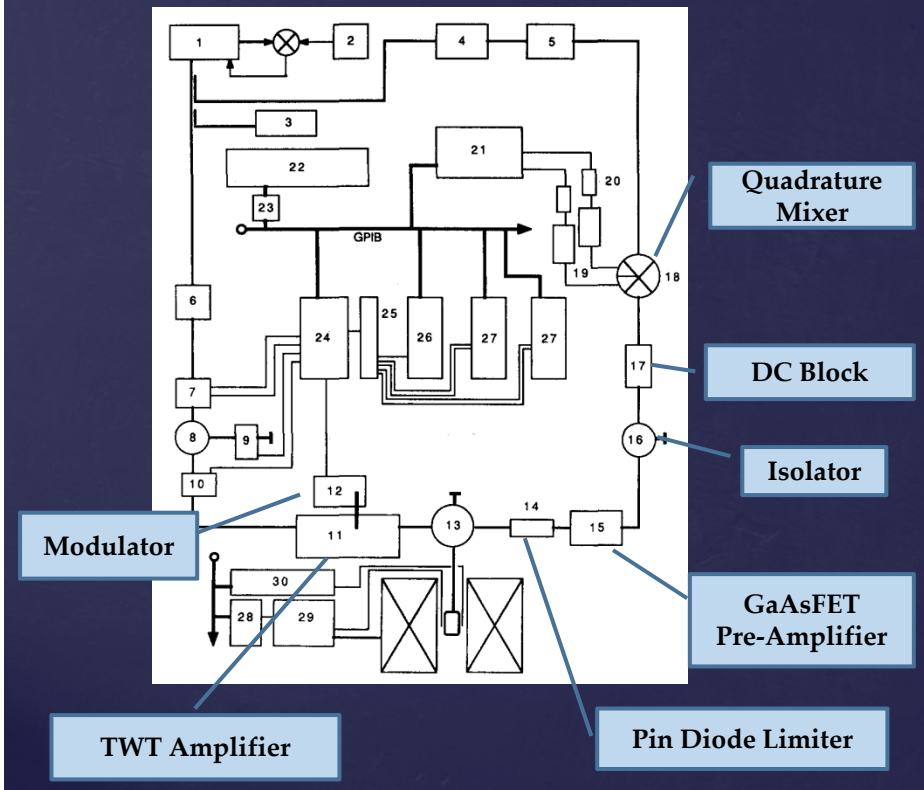

2D-FT-ESR Spectrometer Block Diagram

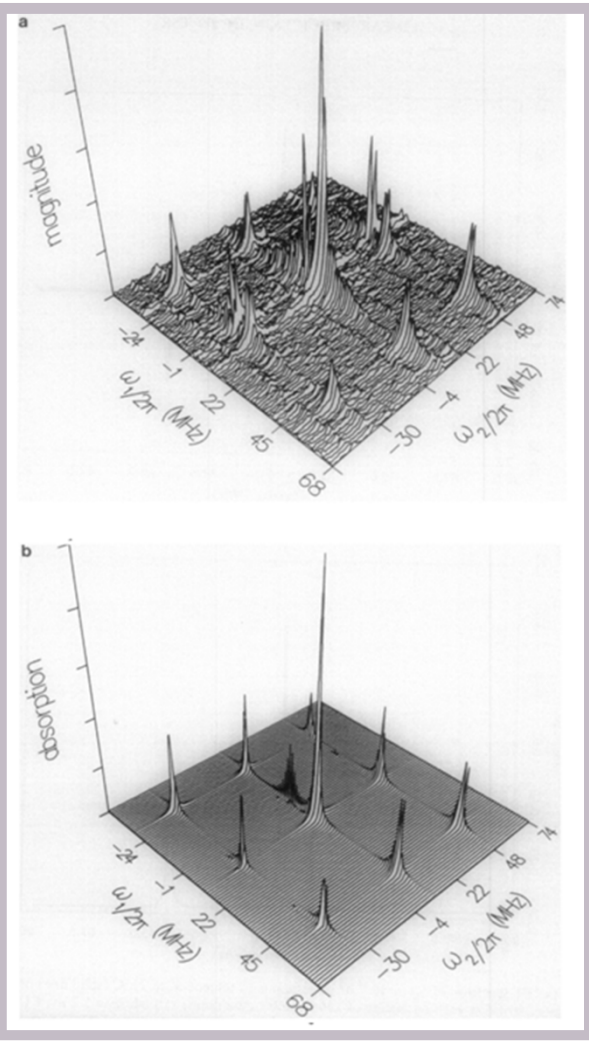

Absolute Value 2-D ELDOR of PD-tempone in toluene-d8 at 21°C. T_{mix}= 3× 10^{-7} s. Cross-peaks due to Heisenberg Spin Exchange.

Spectrum after LPSVD: Pure 2D- Absorption representation.

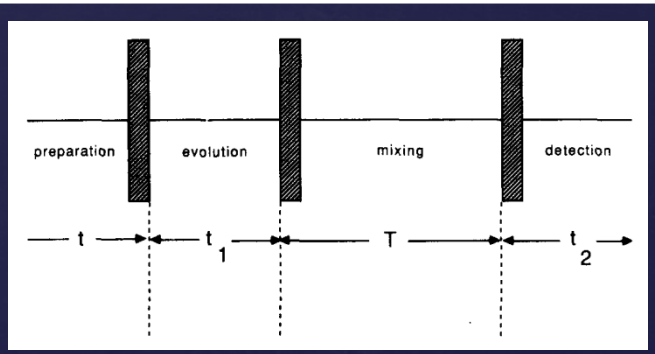

2D-ELDOR pulse sequence: 3 π/2 pulses

1986 cont.

Ultra-High Vacuum ESR (with P.G. Barkley and J.P. Hornak, JCP 84, 1886 (1986)) at 10^{-10} Torr

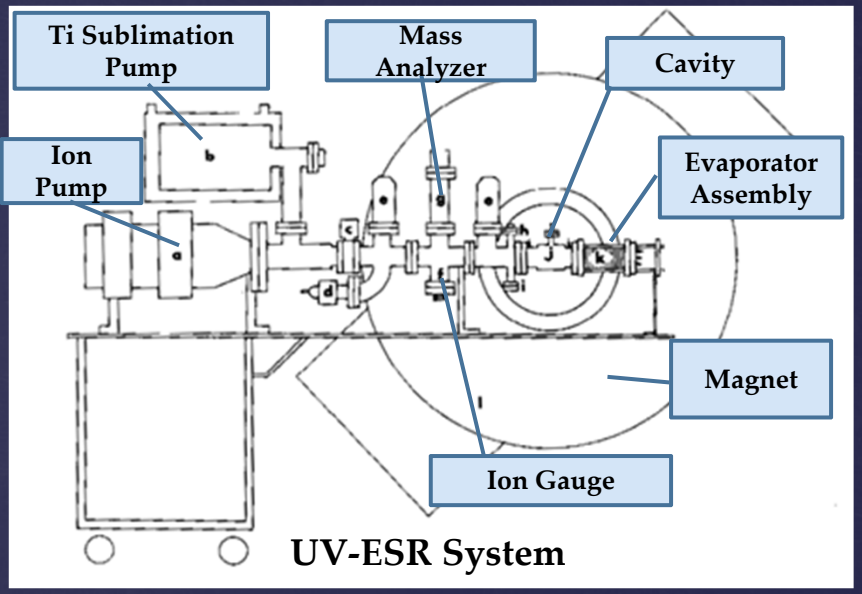

UV-ESR System

UHV-ESR Microwave Cavity
$Q_u \approx$ 13,000, TE011 resonator mode. 50 cm^2 surface area

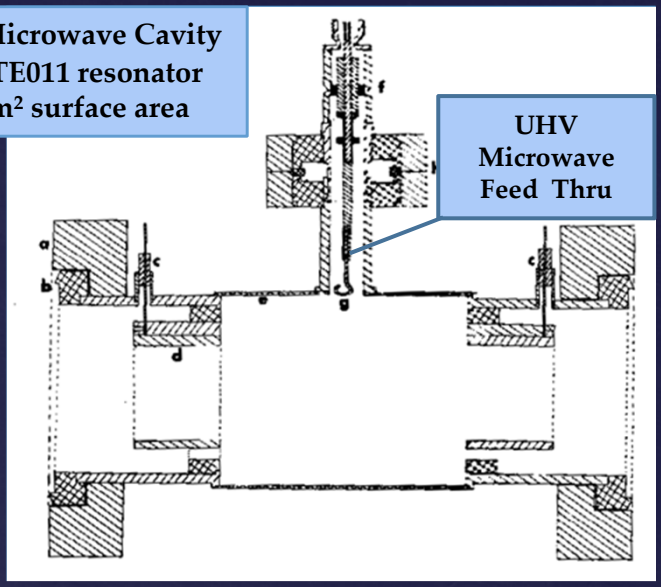

In no case does an ESR signal appear when the nitroxide is first put down on clean Ag or Cu or on the metal pretreated with O_2 (and H_2O). Some minimum dosage is required for ESR signal to be detectable: SSERS (Surface Suppressed Electron Resonance Spectroscopies).

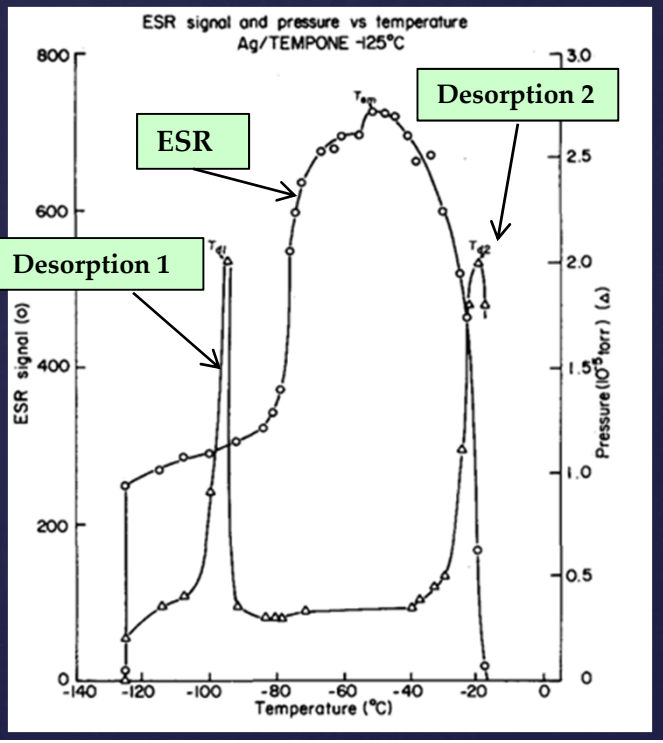

Thermal Desorption Plus ESR Experiment

1989 ISMAR: Morzine, France
JHF: Plenary Lecture

ESR Spectroscopy at 1 MM Wavelengths: FIR-ESR (with B. Lynch & K. Earle, Rev. Sci. Instrum. 59, 1345, (1988))

Fabry-Perot cavity
M indicates mirror assembly

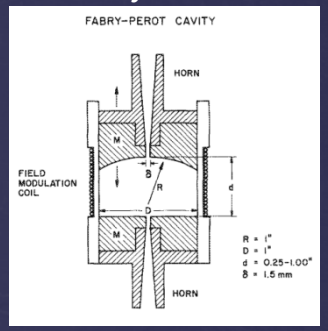

1mm ESR sample holder for low loss samples

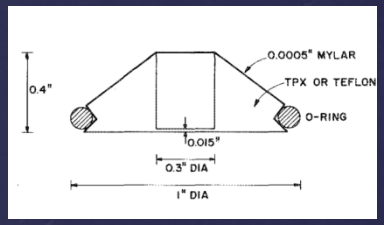

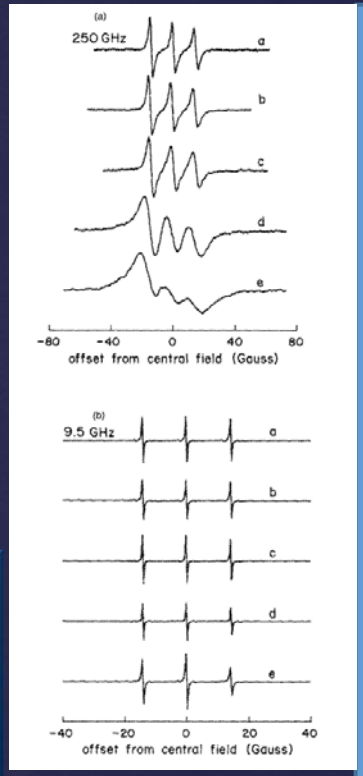

ESR Spectra of PD-Tempone at 250 & 95GHz in solvents of increasing viscosity (a-e).

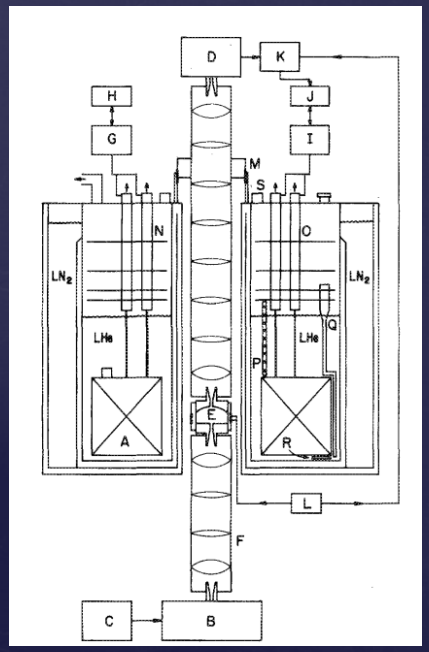

*A motionally narrowed spectrum at 9 GHz looks slow motional at 250 GHz.

Block diagram of 1-mm ESR transmission spectrometer at 9T. using 250 GHz quasi-optical waveguide (OptiguideTM) & 500G-sweep coils.

Quasi-Optical Reflection Bridge 1996 (with* K.A. Earle & D.S. Tipikin, RSI, 67, 2502) Significant Increase in S/N

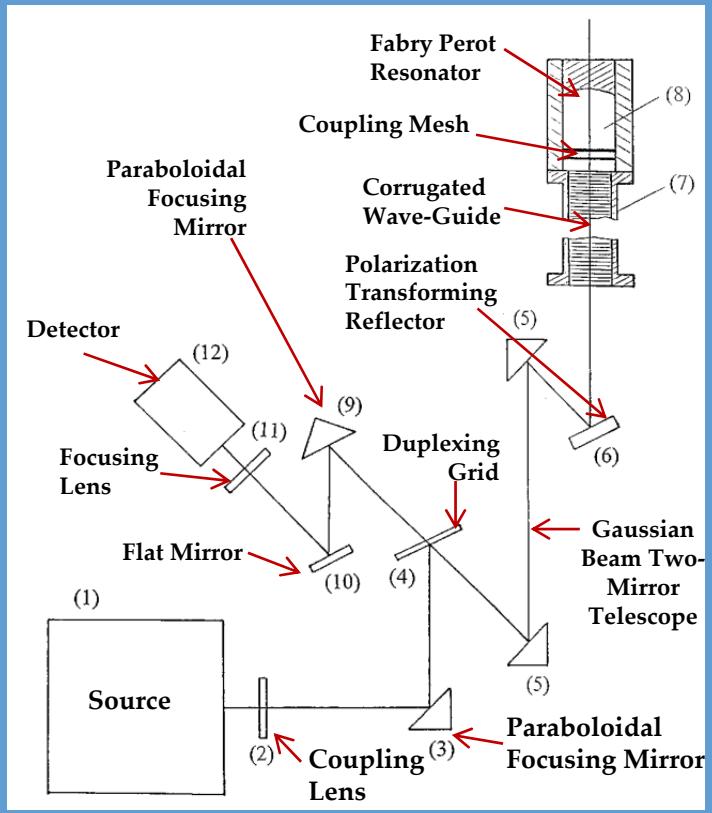

1992 ISMAR: Vancouver, Canada
JHF: Lectured

Diffusion Coefficients in Anisotropic Fluids by ESR Imaging of Concentration Profiles: DID-ESR (with J.P. Hornak, J.K. Moscicki, D.J. Schneider, Y.K. Shin,

Reviewed : Annu. Rev. Biophys. 23, 1 (1994))

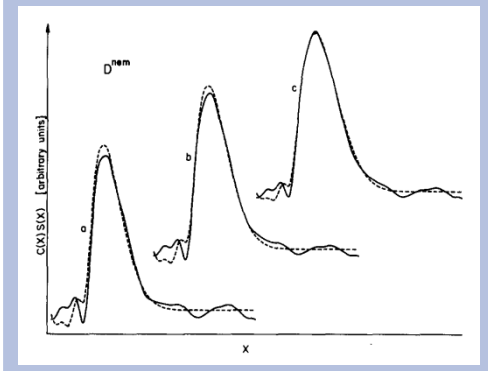

Concentration Profiles for Tempone diffusing in the nematic phase of 5,4 at 300K at increasing times.

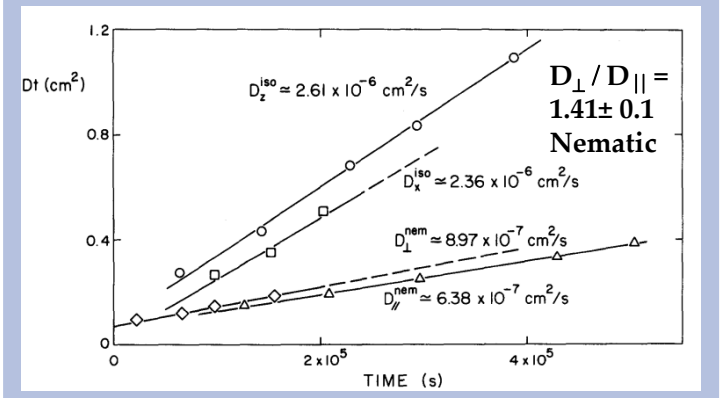

ISOTROPIC/NEMATIC LIQUIDS:
$D_{||} \Rightarrow$ || to Nematic Director.
$D_\perp \Rightarrow \perp$ to Nematic Director

Using 1D field gradients & cw-ESR accurate translational diffusion coefficients ranging from 10^{-5} to 10^{-9} cm²/s were measured in isotropic & anisotropic fluids.

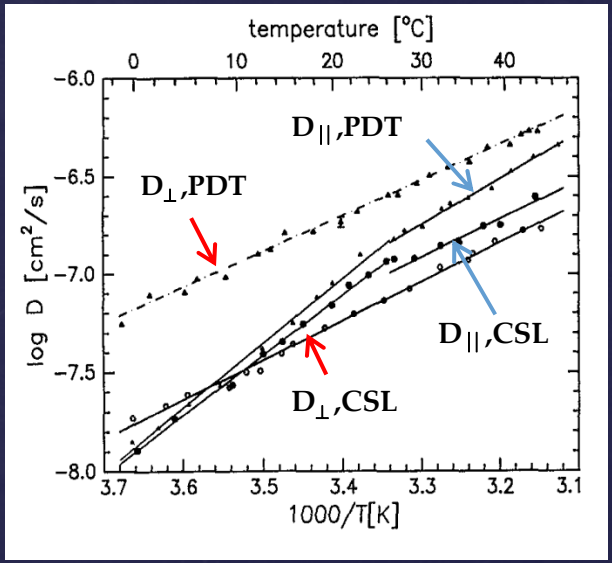

Smectic Liquid Crystal, S2
Small Probe: PDT $D_\perp / D_{||} > 1$
Large Probe: CSL $D_\perp / D_{||} < 1$

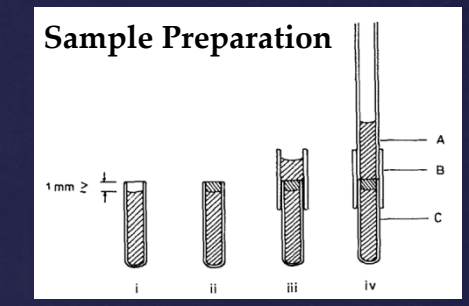

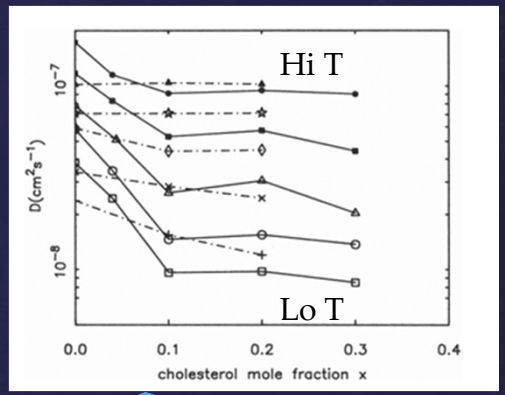

Lateral diffusion of CSL(——) And 16PC (– • – •) in phospholipid POPC vs. cholesterol m.f. at different temperatures

1995: ISMAR: Sidney, Australia
JHF: Session Chm.; Lectured in ESR Satellite

2D-ELDOR & Slow Motions
(with S. Lee, B.R. Patyal, S. Saxena,R.H. Crepeau CPL 221, 397 (1994)) with SRLS Analysis
(with A. Polimeno, JPC, 99, 10995 (1995))

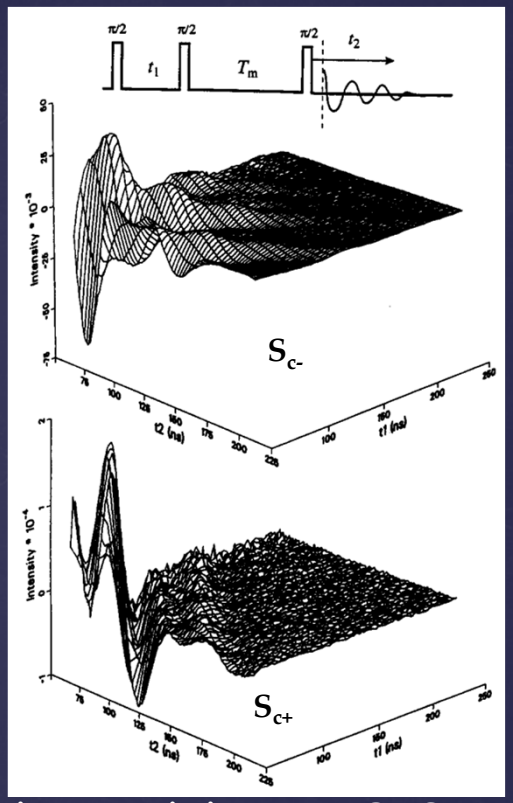

Time Domain in 2D-ELDOR Spectra

The experimental technology for 2D-ELDOR had progressed substantially and the detailed theory based on the SLE was fully developed along with NLLS analysis.

$$S_{c\pm}^{\mathrm{ELDOR}} \propto \langle \nu_{-1} | O_{-1} \exp(-\Lambda_{-1} t_2) O_{-1}^{\mathrm{tr}} P_{(-1\leftarrow 0)} O_0 \times \exp(-\Lambda_0 T_m) O_0^{\mathrm{tr}} P_{(0\leftarrow \mp 1)} O_{\mp 1} \times \exp(-\Lambda_{\mp 1} t_1) O_{\mp 1}^{\mathrm{tr}} | \nu_{\mp 1} \rangle$$

By obtaining 2D-ELDOR spectra at 6-8 different mixing times → actually a 3rd dimension to the experiment.

We found the spin-relaxation and motional dynamics information is very extensive. Simple motional models could not fit data very well, so we applied the SRLS model with considerable success:

In a complex fluid, one expects the molecular reorientation to be non-Markovian. It is modeled in SRLS by both the Smoluchowski-type diffusive rotation of the probe in a mean potential, and the diffusive operator for the reorientation of the local structure (the cage) formed by the molecules in the immediate surroundings of the probe.
Their collective motion constitutes a multi-dimensional Markov process.

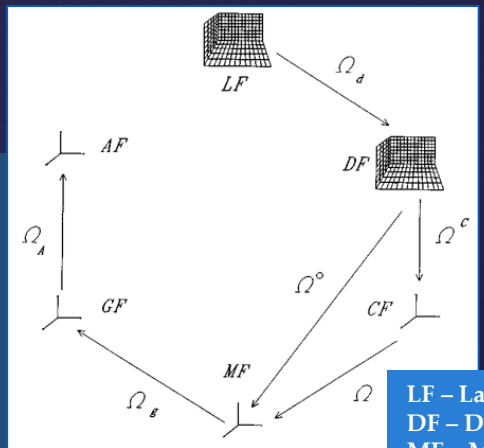

Reference Frames for SRLS

LF – Lab Frame
DF – Director Frame
MF – Molecular Frame
CF – Cage Frame
GF – g-tensor Frame
AF – A tensor Frame

1995 cont.

Multitude of Relaxation and Dynamic Data

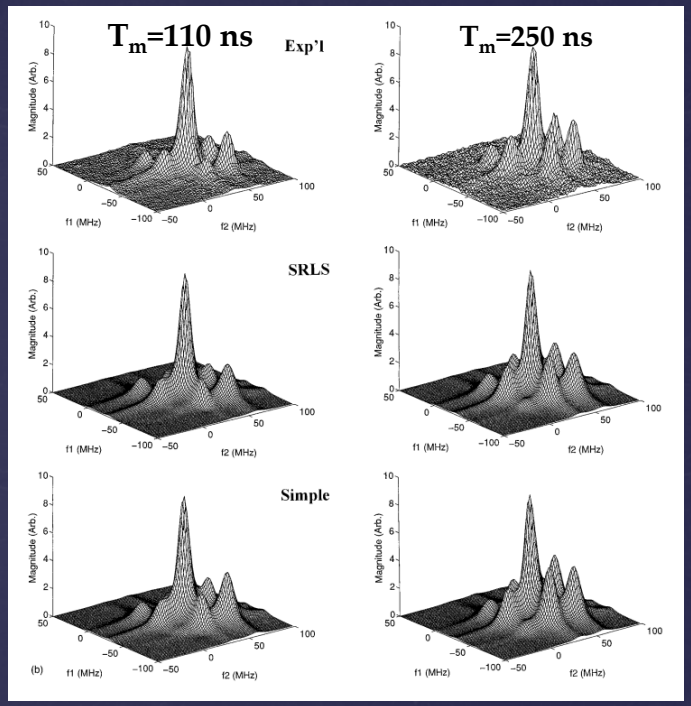

Optimum parameters obtained from fits to the SRLS Model (10 Such Parameters)

Phase	T (°C)	$R_{\parallel}^{o}\times10^{-9}$ (s^{-1})	$R_{\perp}^{o}\times10^{-9}$ (s^{-1})	a_0^2	a_2^2	$T_{1,e}\times10^{6}$ (s)	$T_{2,e}\times10^{6}$ (s)	Δ_G (G)	c_0^2	c_2^2	$R^c\times10^{-7}$ (s^{-1})
I	96.2	0.62	0.119	⋯	⋯	0.068	0.135	1.12	1.10	0.96	2.03
I	91.0	0.57	0.094	⋯	⋯	0.077	0.152	1.07	1.04	0.95	0.90
I	86.1	0.53	0.088	⋯	⋯	0.072	0.188	1.15	0.69	1.00	0.43
I	80.2	0.49	0.080	⋯	⋯	0.110	0.187	1.02	0.73	0.96	0.48
N	73.1	0.77	0.138	1.93	1.46	0.582	0.095	0.86	1.85	0.62	1.08
N	70.2	0.68	0.131	2.15	0.86	0.582	0.111	0.93	2.00	0.62	1.40
N	67.5	0.65	0.121	2.50	1.12	0.582	0.122	0.82	1.84	0.81	1.01
N	65.0	0.54	0.101	2.74	1.27	0.582	0.138	0.80	1.72	0.62	0.84
S_A	59.1	2.37	0.081	3.57	0.84	0.288	0.283	0.94	2.26	0.82	0.33
S_A	56.4	2.36	0.086	3.79	1.16	0.359	0.343	1.01	2.23	0.78	0.32
S_A	53.6	2.48	0.077	4.15	1.44	0.478	0.442	1.11	2.25	0.79	0.33
S_A	50.8	2.33	0.083	4.68	1.17	0.316	0.196	1.28	1.62	0.74	0.28
S_B	44.4	3.23	0.150	7.49	−0.62	0.185	0.092	1.19	0.215	−0.029	0.022
S_B	40.7	2.86	0.115	7.78	−0.50	0.178	0.098	1.19	0.191	−0.003	0.021
S_B	38.1	2.77	0.150	7.55	−0.58	0.206	0.095	1.21	0.246	−0.010	0.022
S_B	35.2	2.09	0.141	7.62	−0.88	0.216	0.103	1.23	0.451	−0.027	0.015
C	29.1	2.00	0.124	7.61	−0.86	0.216	0.108	1.23	0.200	−0.004	0.010
C	24.6	1.98	0.137	7.96	−1.40	0.216	0.116	1.23	0.075	−0.002	0.000

[a]The average percent errors to the parameters are $\epsilon_{R_{\parallel}^{0}}=1.5$, $\epsilon_{R_{\perp}^{0}}=2.7$, $\epsilon_{a_0^2}=1.8$, $\epsilon_{a_2^2}=1.1$, $\epsilon_{T_{1,e}}=2.5$, $\epsilon_{T_{2,e}}=5.0$, $\epsilon_{\Delta_G}=1.6$, $\epsilon_{c_0^2}=2.5$, $\epsilon_{c_2^2}=2.7$, $\epsilon_{R^c}=3.7$.

CSL in Macroscopically Aligned Smectic A phase of Liquid Crystal 40.8 (59°C).
(V.S.S. Sastry, et al., JCP 105, 5753 (1996))

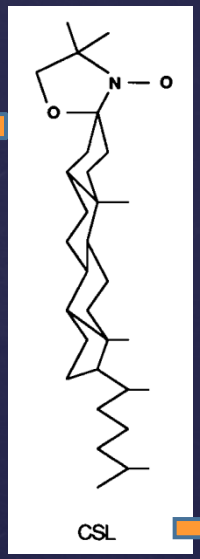

CSL In Liquid Crystalline Polymer
D. Xu et al. (JPC 1001, 15873 (1996)

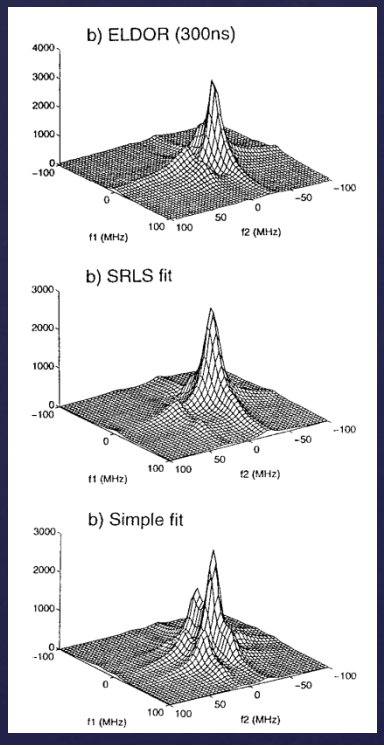

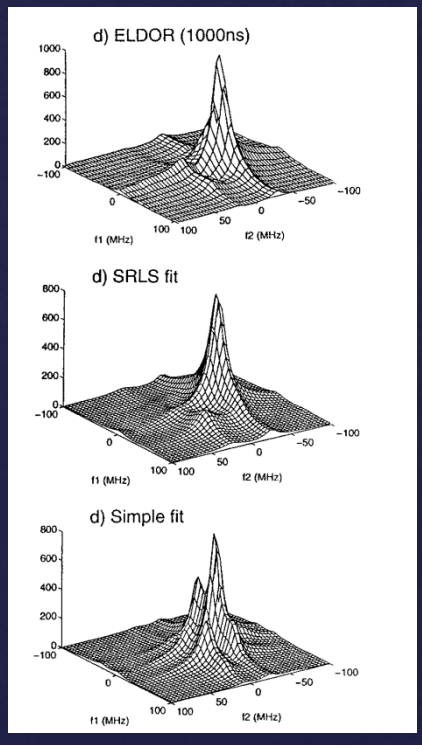

1998: ISMAR: Berlin, Germany
JHF: Lectured

250 GHz Studies of Molecular Dynamics

1) Dynamic Cage Effects Above the Glass Transition (with K. Earle, J.K. Moscicki, A. Polimeno, JCP, 106, 9996, (1997))

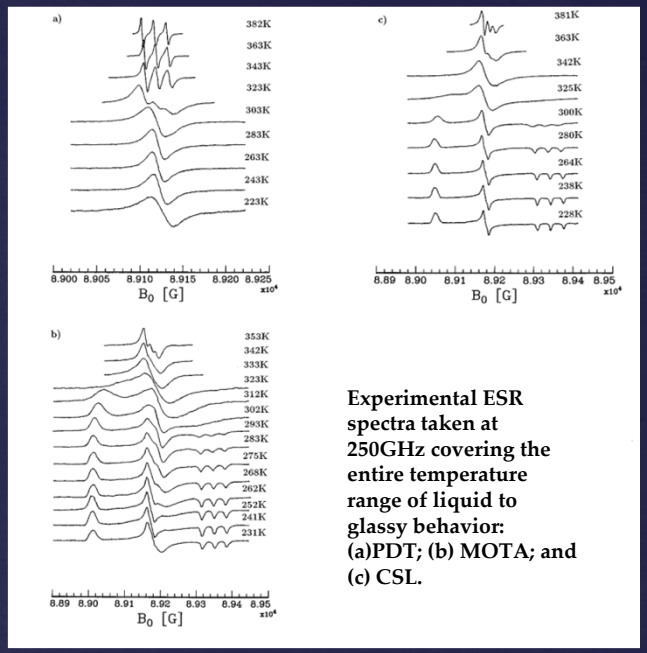

Experimental ESR spectra taken at 250GHz covering the entire temperature range of liquid to glassy behavior: (a)PDT; (b) MOTA; and (c) CSL.

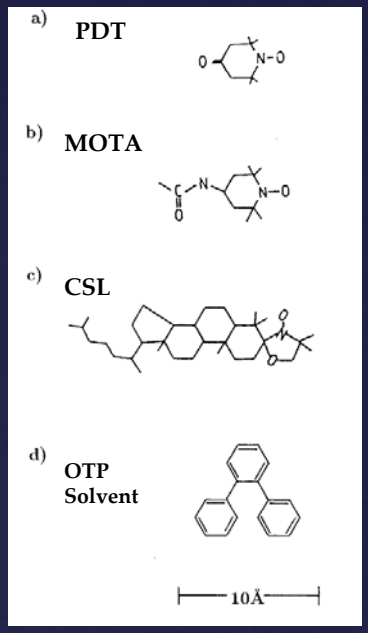

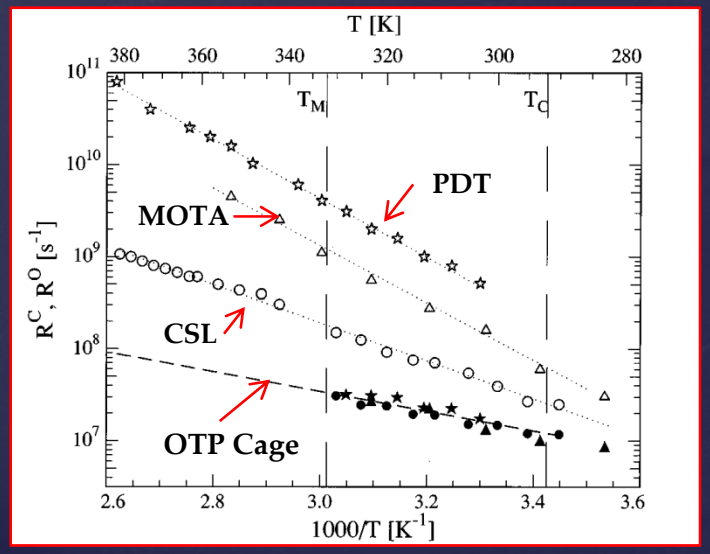

Rotational Diffusion Rates for Probes dependent upon their size.
Relaxation of cage is the same for all the probes.

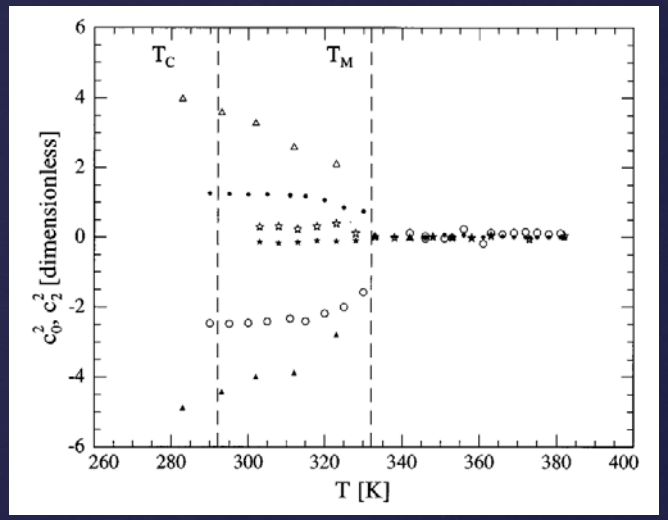

Cage potential parameters below T_M depend on size and shape of probe; above T_M they all are zero.

2001: ISMAR: Rhodes

JHF: Lectured; ACERT is initiated.

Protein Structure Determination Using Long-Distance Constraints from Double-Quantum Coherence (DQC) ESR: T4–Lysozyme (with Peter Borbat* & H.S. Mchaourab , JACS 124, 5304 (2002))

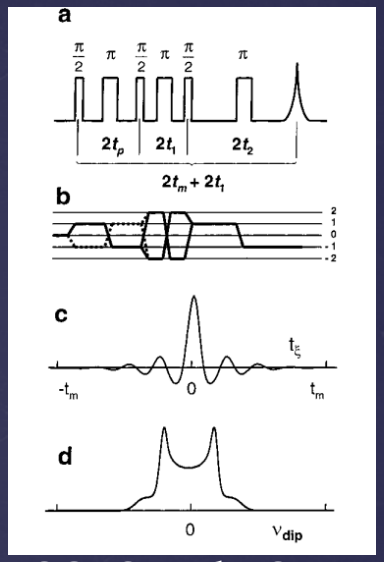

DQC-ESR Pulse Sequence

π/2 pulses = 3.2 ns

π pulses = 6.4 ns

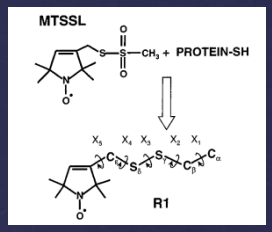

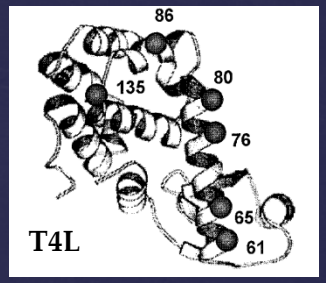

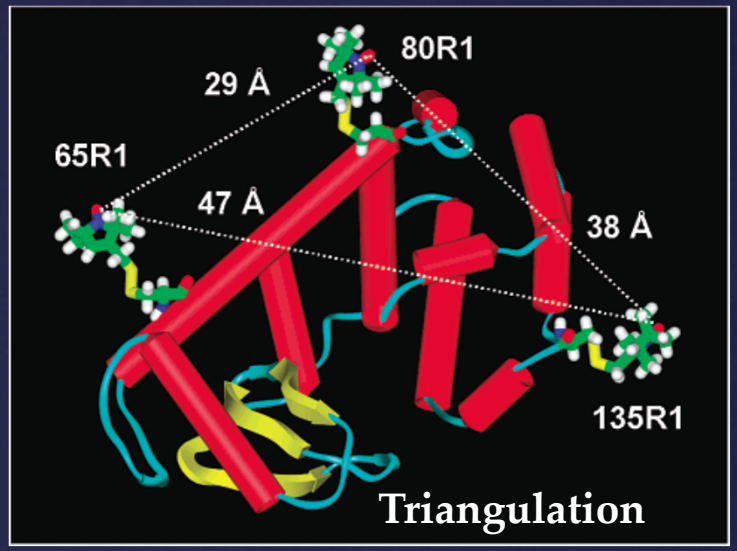

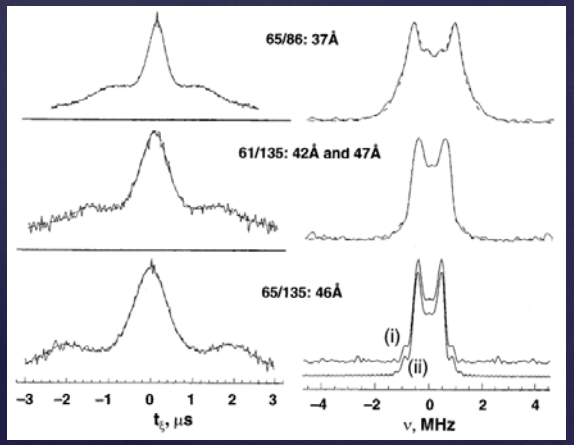

Left: Time evolution of DQC Signal from doubly labeled T4L; Right : their FT's

Table 3. Comparisons of Average Distances between Nitroxides, R_{av}, from the DQC Experiments (cf. Table 2) with the Distances, $R_{\alpha\alpha}$ and $R_{\beta\beta}$, between the Respective α- and β-Carbons, Obtained from X-ray Crystallography[60]

mutant	R_{av}, Å	$R_{\alpha\alpha}$, Å	$R_{\beta\beta}$, Å	Δ^a, Å
61/80	34, 29	28.7	28.82	5.3, 0
65/80	28.0[b]	22.6	22.4	5
65/76	21.4	16.7	16.6	4.7
61/86	37.5, 33.5	34.4	37	3, 0.9
65/86	37.4	28.86	31.17	8.5
61/135	47.2, 41.8	37.7	40.43	9.5, 4
65/135	46.3	34.26	36.67	12
80/135	36.8	26.7	27.4	10

[a] $\Delta \equiv R_{av} - R_{\alpha\alpha}$. [b] Average of distances from X- and Ku-bands.

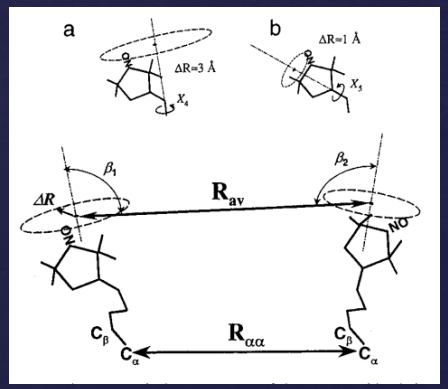

Accounting for Flexibility of Tether

2001 Cont.

Dipolar Relaxation in a Many-Body System of Spins of ½: Translation Diffusion (with A.A. Nevzorov, JCP, 112, 1425 (2000); 115, 2401 (2001))

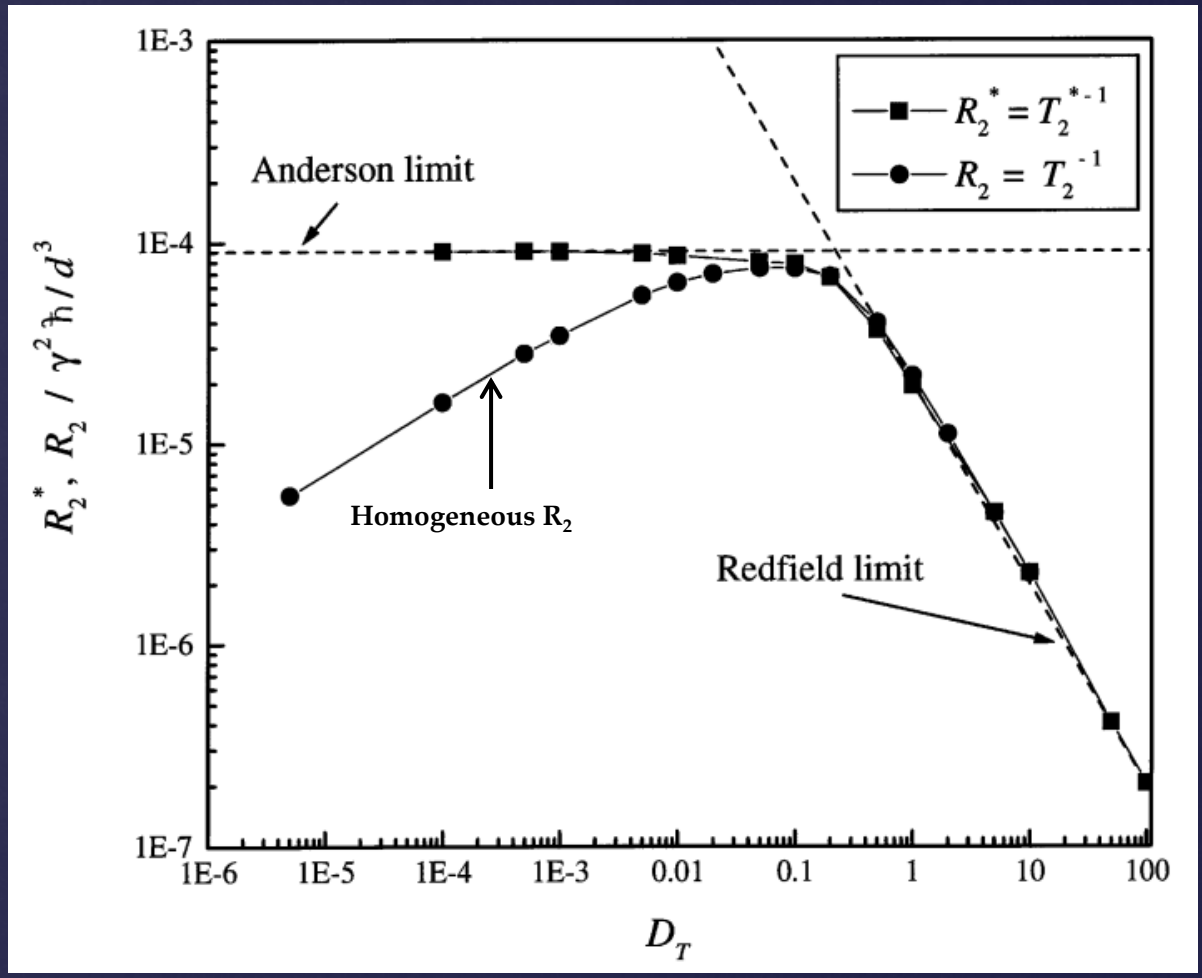

Bridging the two limits vs. relative translational diffusion coefficient D_T

2004 ISMAR: Jacksonville, FL (USA)
JHF: Plenary Lecture

95 GHzHigh-Power Quasi-Optical Pulsed ESR Spectrometer (with* W. Hofbauer, K.A. Earle, C.R. Dunnam, J.K. Moscicki, RSI 75, 1194 (2004))

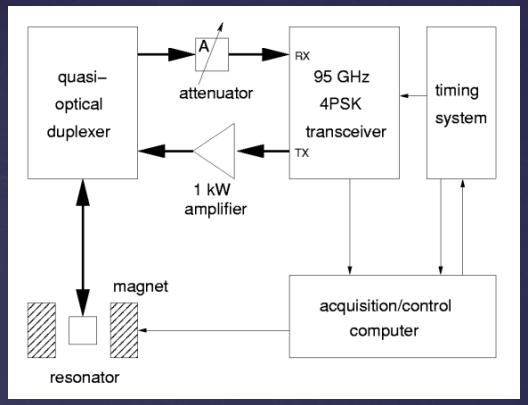

Spectrometer Block Diagram

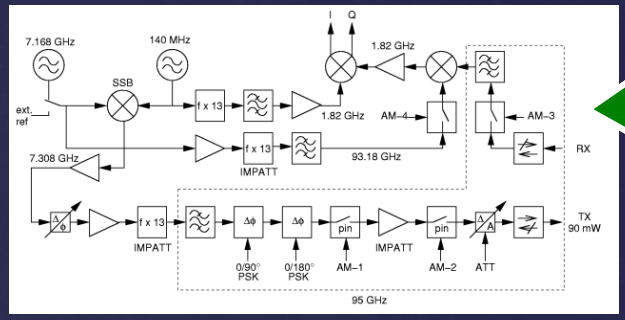

Block Diagram of Transceiver
5ns $\pi/2$ pulse ≅ 18 G.
Spectral bandwidth
± 175 MHz (or ± 62 G.)

Schematic Diagram of Quasi-Optical Bridge Based on Polarization Coding: Induction Mode.

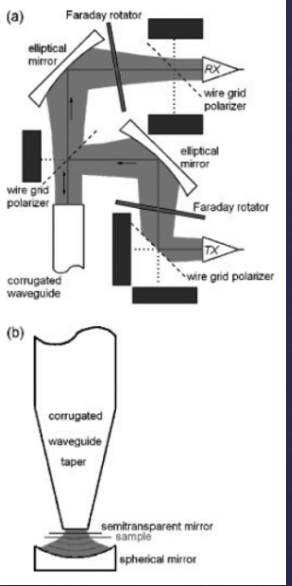

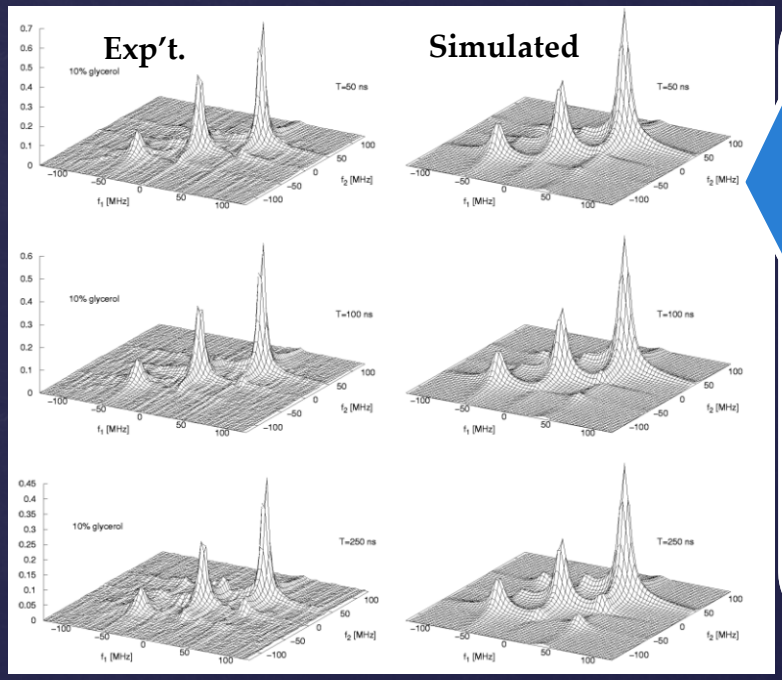

2-D ELDOR, Sc- Spectra of Tempo in 90% water/10% glycerol, 22°C at various mixing times.

New relaxation mechanism ineffective at lower fields & frequencies. e.g. dynamic modulation of the g-value due to rapid solvent-induced fluctuations.

2004 Cont.

Electron Spin Resonance Microscopy: Micron Resolution (with A. Blank*, C.R. Dunnam, P.P. Borbat, RSI 75, 3050; APL 85, 5430 (2004))

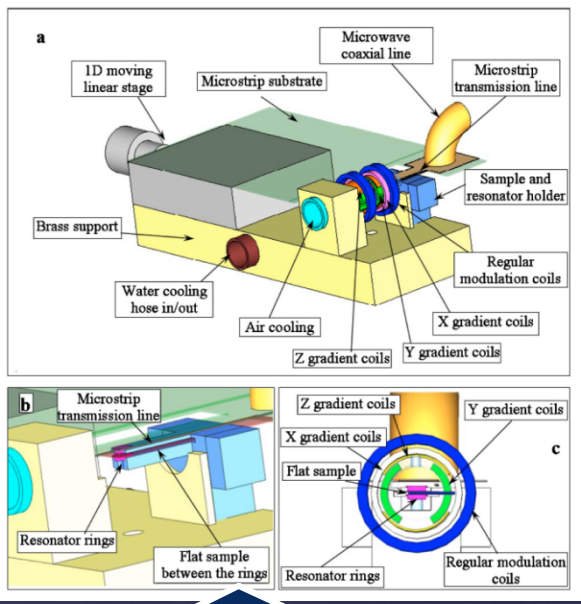

CW Imaging Probe Layout

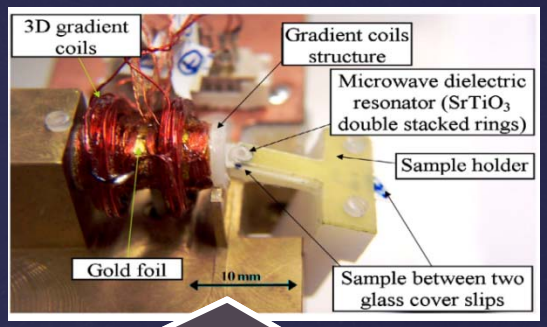

Photo of Pulsed Imaging Probe

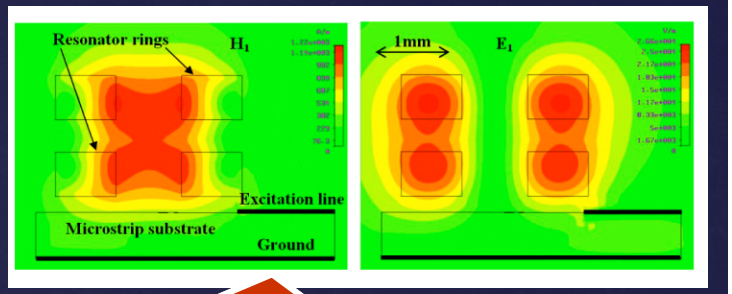

Calculated Microwave H_1 & E_1 fields for High Permitivity Resonator

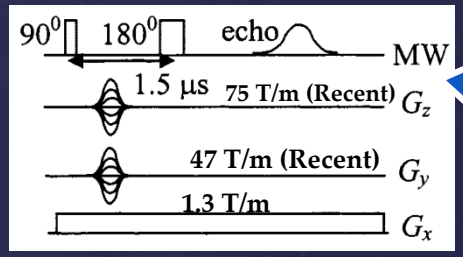

Typical Pulse Imaging Sequence

Imaging Mouse Leg Tissue with tumor (2010)

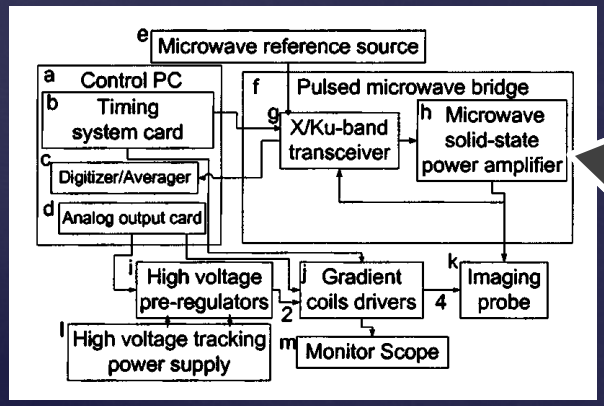

Block Diagram of the Pulsed Imaging System

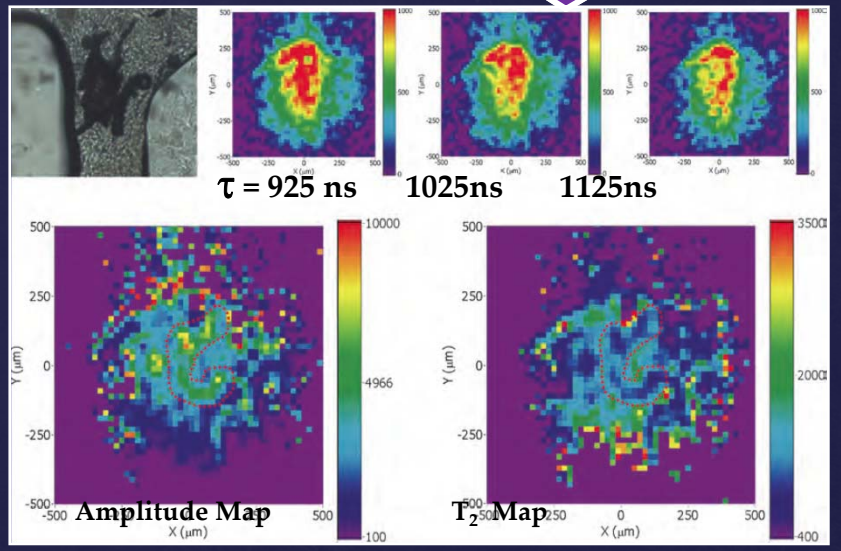

LiPc crystal size of 55 X 67 X 15 µm
Recent ESRM ~ 0.7 X 0.75 X 7.5 µm

2007: ISMAR: Taiwan
JHF: Lectured

Dynamic Molecular Structure of Phase Domains in Model & Biological Membranes by 2D-ELDOR with the "Full Sc- Method" (with Y.-W. Chiang, A.J. Costa-Filho, JPC-B, 111, 11260 (2007))

The Sc- method is a newer fitting strategy using the full complex Sc- signal instead of just the magnitude.

(Note the FID-like Sc+ signal is heavily attenuated due to finite-dead times, ca. 30 ns.).

Excellent discrimination of the three phases of mixed model membranes of DPPC/Cholesterol with 16 PC

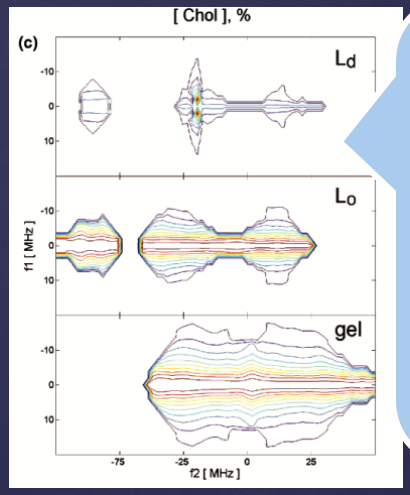

Absoption Spectra in Normalized Contour Mode: Shows Homogeneous Linewidths.

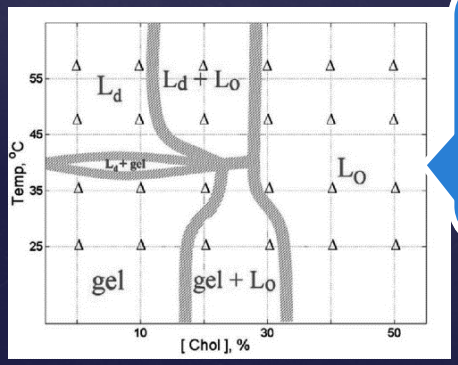

Yields this Phase Diagram

Pure Absorption Components for coexisting Lo & Ld phases in plasma membrane vesicles

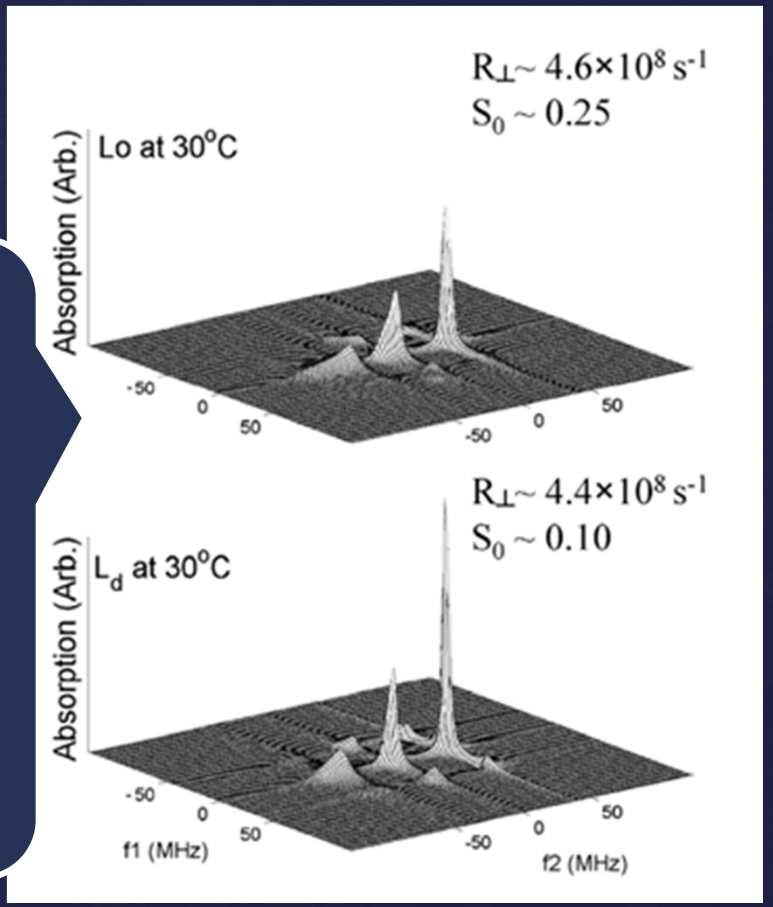

2007 Cont.

Multi-Frequency ESR and Molecular Dynamics in Biophysical Systems (with Z. Zhang, M.R. Fleissner, D.S. Tipikin, Z. Liang, J.K. Moscicki, Y. Lou, M. Ge, and W. Hubbell).

Provides extensive experimental data to study microscopics of molecular dynamics. The multi-frequency ESR studies to date cannot be adequately fit with simpler models, but require the SRLS model, which provides adequate fit.

Complex Dynamics of Membranes

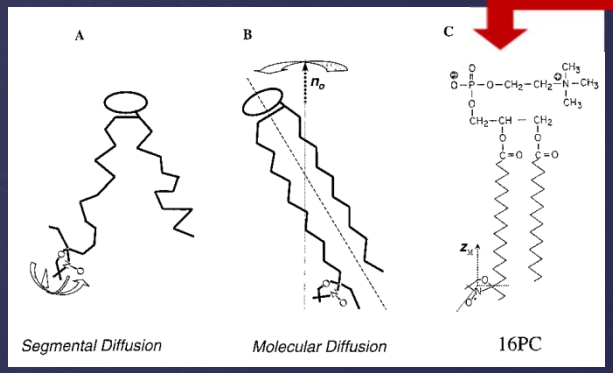

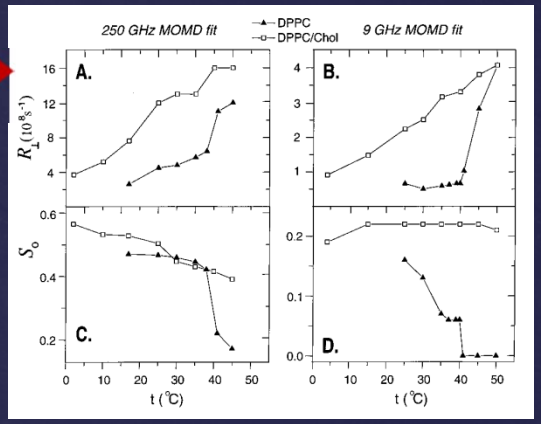

Standard MOMD fits are in disagreement. Only by the SRLS analysis could results at both frequencies be fit simultaneously & with physically sound axial alignment of the acyl chains.

Complex Dynamics of Spin-Labeled T4 Lysozyme

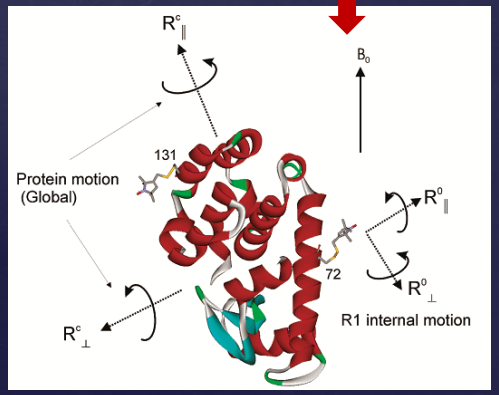

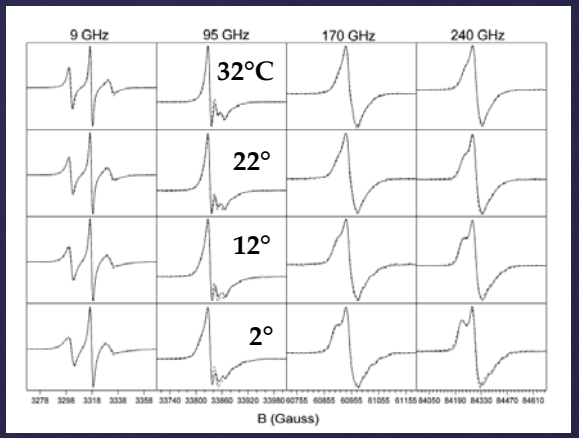

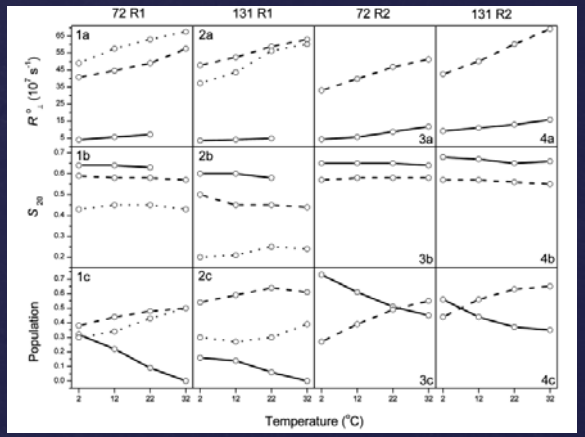

Spectra At 4 Frequencies Were Fit Simultaneously To SRLS. Yields 3 Distinct Components

2010: ISMAR: Florence Italy
JHF: Lectured

Protein Superstructure: Bridging the Gap Between X-ray Crystallography and Cyro-EM by Pulse-Dipolar ESR (with J. Bhatnagar, P. Borbat, A. Pollard, A. Bilwes, B.R. Crane, Biochem. 49, 3824 (2010))

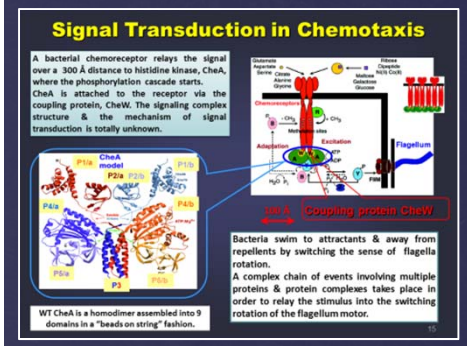

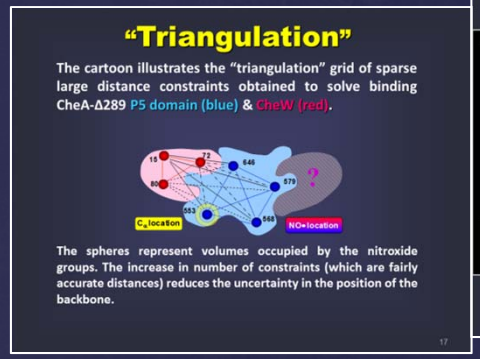

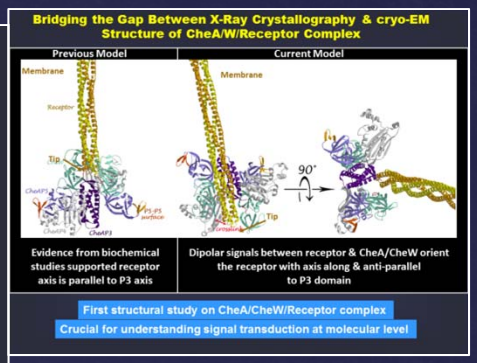

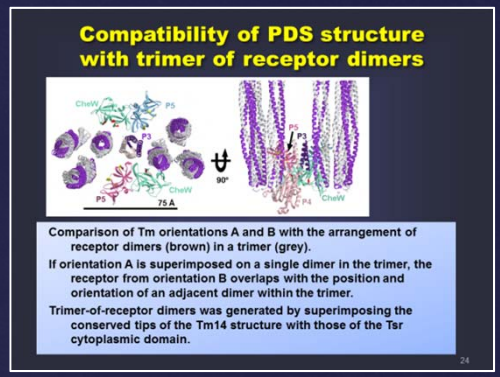

Structureless Protein Which Binds to Membranes: α – Synuclein (with E.R. Georgieva, T.F. Ramlall, P. Borbat, D. Eliezer, JBC, 285 , 28261 (2010))

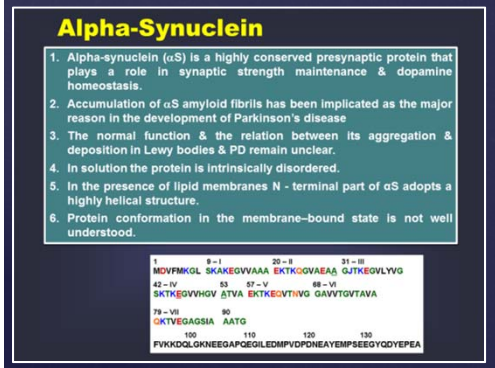

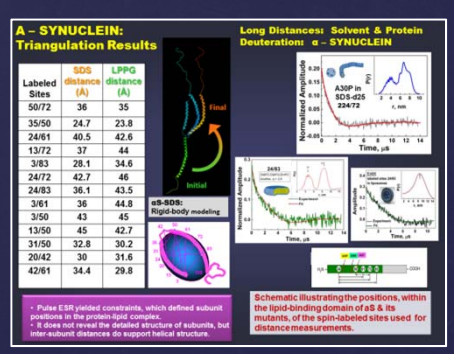

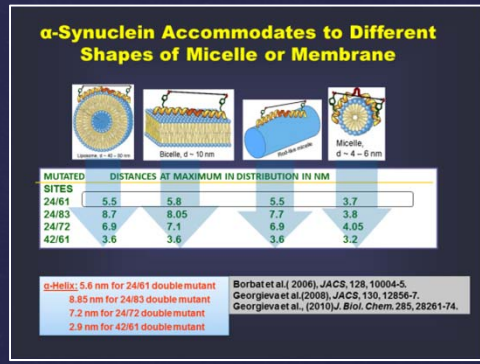

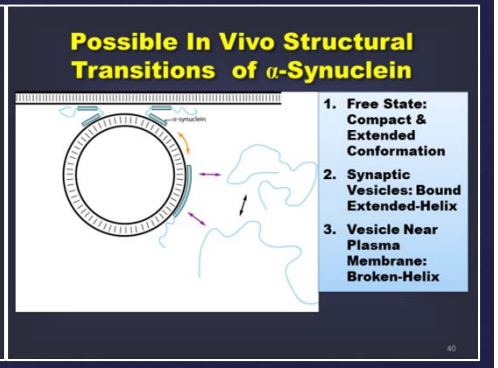

2013: ISMAR: Rio de Janiero, Brazil
JHF: ISMAR Prize, Lecture

Sensitivity of Pulse Dipolar ESR at ACERT (with P.P. Borbat*, JPC Letters, 4, 170 (2013))

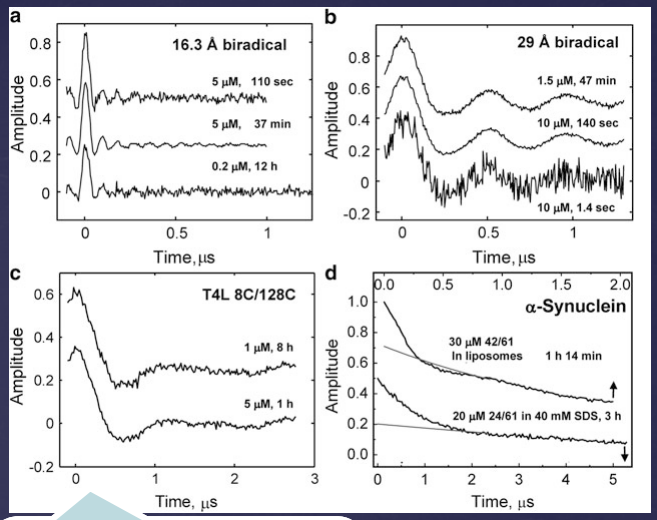

Micromolar Concentration Sensitivity with DEER: ACERT:Ku Band

5-Pulse DEER (Borbat) can nearly double dipolar evolution times. Good for longer distances

π/2, π, π/2,π, π/2, π

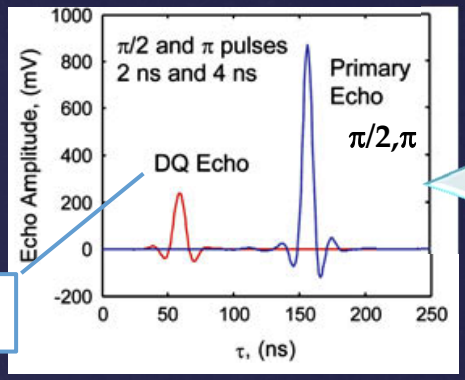

DQC Signal is 52% of theoretical maximum; Half of primary echo

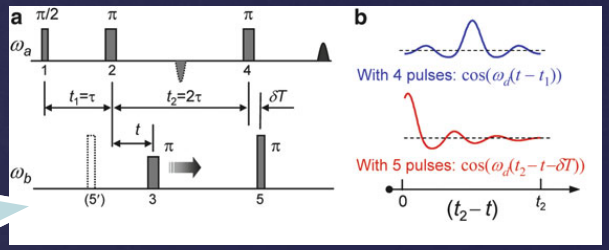

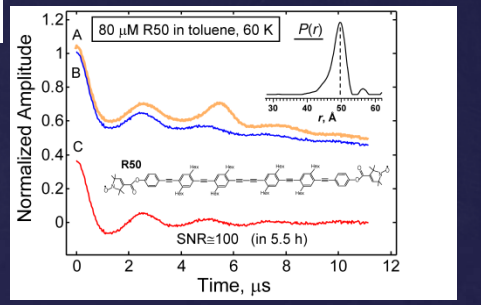

Locating a lipid in a Macromolecular Complex (with B. Gaffney, M.D. Bradshaw, S.D. Fausto, F. Wu, P. Borbat, BJ, 103, 2134 (2012))

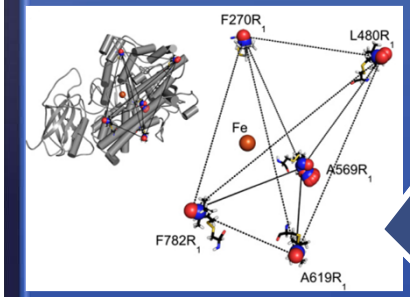

Protein Grid from 10 Distances between 5 spin-labeled sites on lipoxygenase

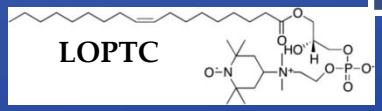

Distance Geometry approach assigned the location of the polar end of LOPTC on protein surface to 2σ < 2 Å accuracy

Distances of LOPTC to the 5 sites on protein

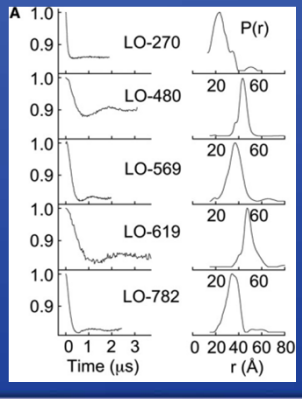

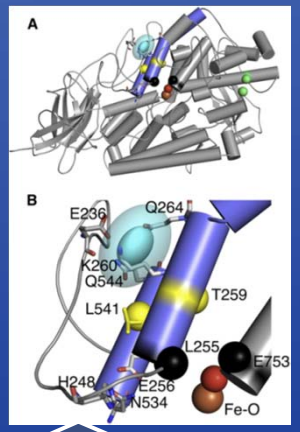

Locating LOPTC in the Protein

2013 Cont.

Conformational Ensemble of sodium-coupled aspartate transporter (with Elka R. Georgieva, P.P. Borbat, C. Ginter, O. Boudker, NSMB, 20, 215 (2013))

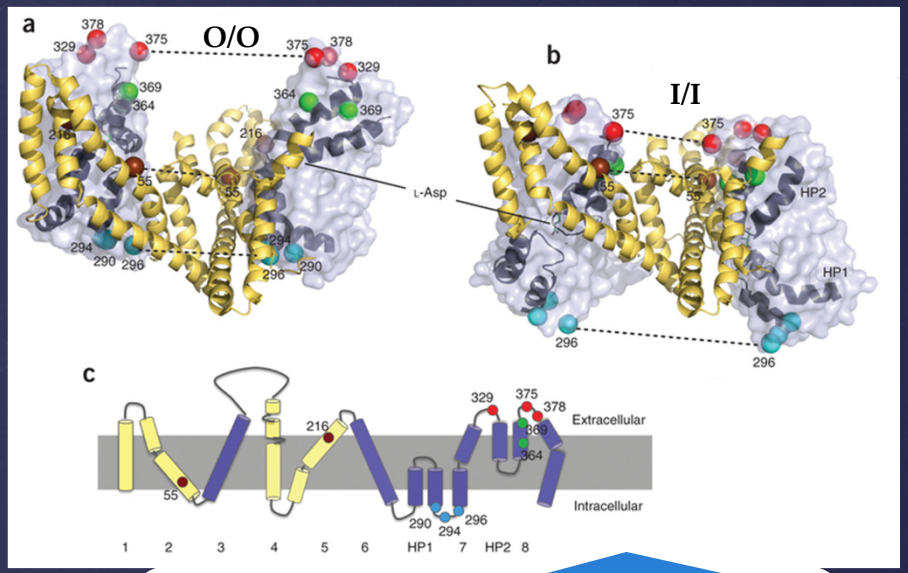

Trimer Transporter

a) Protomer pairs in outward-facing state
b) Pairs in inward-facing state
c) Topology of protomer

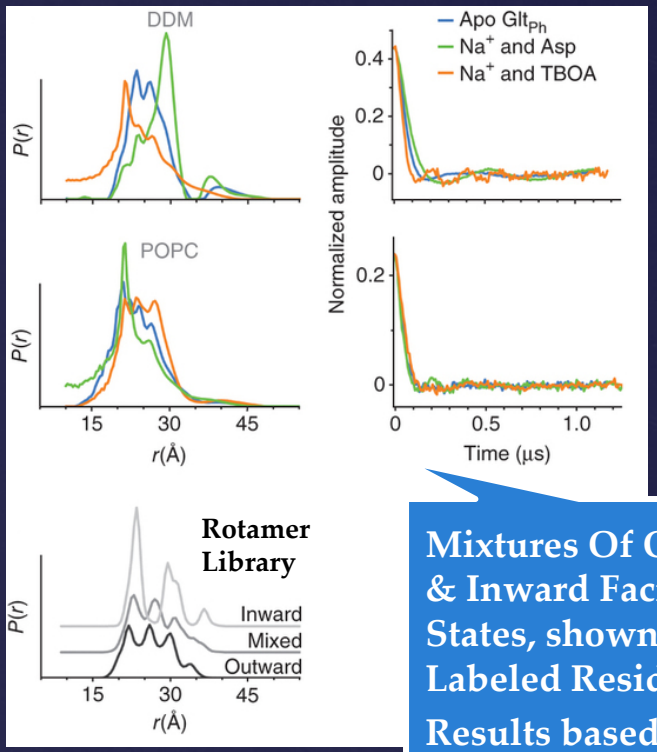

Mixtures Of Outward & Inward Facing States, shown for Labeled Residue 55.

Results based on 139 Distances

Found: Outward & Inward States With Nearly Equal Probability Indicative Of Comparable Energies & Protomers Function Independently Of Each Other.

Structure Of Protomers In Membrane More Compact Than In Detergent, Yet Consistent With Crystal Structures.

I hope this excursion through my 51 years of ESR has given some indications of how this field of magnetic resonance has evolved with many exciting capabilities.